Boada, B. L., Viadero-Monasterio, F., Zhang, H. & Boada, M. J. L. (2022). Simultaneous Estimation of Vehicle Sideslip and Roll Angles Using an Integral-Based Event-Triggered Hinfinity Observer Considering Intravehicle Communications *IEEE Transactions on Vehicular Technology*, 1-15.

DOI: 10.1109/tvt.2022.3222866

Simultaneous Estimation of Vehicle Sideslip and Roll Angles Using an Integral-Based Event-Triggered H_∞ Observer Considering Intravehicle Communications

Beatriz L. Boada, Fernando Viadero-Monasterio, Hui Zhang, and Maria Jesus L. Boada

***Abstract*—In recent years, several technological advances have been incorporated into vehicles to ensure their safety and ride comfort. Most of these driver-assistance technologies aim to prevent skidding, whereas less attention has been paid to the avoidance of other dangerous situations such as a rollover. Since knowledge of slip and roll angles is critical to the control and safety of vehicle handling, their estimation remains of great interest when addressing emerging constraints in modern technologies involving networked communications and distributed computing. This paper presents an integral-based event-triggered H_∞ observer to simultaneously estimate the sideslip and roll angles, considering intravehicle communications with a networked-induced delay. As the longitudinal velocity and tire cornering stiffness of a vehicle can vary significantly during driving and have a strong influence on vehicle lateral stability, these time-varying parameter uncertainties are considered in the design of the observer. The simulation and experimental results demonstrate the effectiveness of the proposed observer.**

***Index Terms*—Integral-based event-triggering, intravehicle communication, networked-induced delay, parameter uncertainties, H_∞ performance, sideslip and roll angle estimation.**

I. Introduction

In recent years, several technological advances have been incorporated into vehicles to ensure their safety and ride comfort. These systems, which have traditionally been developed to help drivers handle the vehicle, play a key role in the emerging trend of autonomous vehicles (AVs). In relation to the handling stability of a vehicle, lateral and yaw stability control are major concerns [1]–[6]. Most of these driver-assistance technologies aim to prevent skidding of vehicles, whereas less attention has been paid to the avoidance of other dangerous situations such as a rollover, which occurs mainly in vehicles with high center of gravity (CoG) or low roll stiffness [7], [8]. An adequate design of advanced driver-assistance systems entails an accurate and full knowledge of the vehicle states. In this regard, the sideslip angle and the roll angle are required to enhance the lateral and roll stability performance, respectively [9]. These angles can be measured directly by using sensors such as the Correvit S-Motion DTI from Kistler or VBOX 3i dual antenna from Racelogic, among others. The main drawback of these sensors is that they are very expensive, making it infeasible to mount them on current series-production vehicles. The best solution proposed so far is to estimate the sideslip and roll angles based on dynamical models of the vehicle using measurements obtained by sensors already installed in most vehicles or by low-cost sensors [10]–[12].

Most previous works have focused on estimating one or the other angle, mainly the sideslip angle [13]. Di Biase et al. [14] proposed a novel vehicle sideslip angle estimator consisting of a simple single-stage extended Kalman filter (EKF) approach for a heavy-duty vehicle using a rational tyre model. Villano et al. [15] proposed the development of an unscented Kalman filter (UKF) framework based on an innovative combination of kinematic and dynamic modeling, called a cross-combined approach, for vehicle sideslip angle estimation using measurements from sensors already available on many of today's passengers vehicles. Unfortunately, the lateral and roll dynamics of a vehicle are heavily coupled [16], so the simultaneously estimation of roll and sideslip angles should be performed. Cho et al. [17] proposed an observer based on a bicycle model combined with a kinematic model that uses lateral acceleration information. Additionally, a new roll angle estimation methodology was proposed to compensate the issue of drift in the lateral accelerometer used directly for the observer. Hac et al. [18] used kinematic based-models that consider the motion of a body and that are not affected by uncertainties to estimate both the roll and sideslip angle. Nevertheless, unexpected disturbances and model uncertainties should be considering to guarantee a robust estimation in different situations.

Since knowledge of the sideslip and roll angles is critical for vehicle handling and safety control, their estimation continues to arouse great interest, especially to deal with the limitations

Beatriz L. Boada is with the Department of Mechanical Engineering and also with the Research Institute of Vehicle Safety (ISVA), University Carlos III de Madrid, Avda. de la Universidad, 30, 28911, Leganes, Madrid, Spain (e-mail: bboada@ing.uc3m.es).

Fernando Viadero-Monasterio is with the Department of Mechanical Engineering, University Carlos III de Madrid, Avda. de la Universidad, 30, 28911, Leganes, Madrid, Spain (e-mail: fviadero@ing.uc3m.es).

Hui Zhang is with the School of Transportation Science and Engineering, Beihang University, Beijing 100091, China and also with the Ningbo Institute of Technology (NIT), Beihang University, Ningbo 315323, China (e-mail: huizhang285@buaa.edu.cn).

Maria Jesus L. Boada is with the Department of Mechanical Engineering and also with the Research Institute of Vehicle Safety (ISVA), University Carlos III de Madrid, Avda. de la Universidad, 30, 28911, Leganes, Madrid, Spain (e-mail: mjboada@ing.uc3m.es).

Manuscript received April XX, 2021; revised August XX, 2021.This work was supported by the FEDER/Ministry of Science and Innovation - Agencia Estatal de Investigacion (AEI) of the Government of Spain through the project RTI2018-095143-B-C21.

and problems that arise with the improvement of modern control technologies embedded in electronic control systems [19] involving networked communications and distributed computing. The continuous and rapid development of more advanced vehicular applications and devices implies the coexistence of different vehicular communication networks [20], [21], both intra- and intervehicle. In intravehicle networks, the devices (sensors and actuators) are connected to computing modules through either wired or wireless communication to facilitate the operation of a single vehicle [22], [23]. Meanwhile, intervehicle networks allow information exchange from vehicle to vehicle (V2V) and between vehicles and infrastructure (V2I). The latter type of network uses shared service platforms and cloud computing to reduce the information storage requirements and the computational burden om the vehicle's onboard resources [24]. Nevertheless, Milano et al. [25] state that those functions that are crucial for the normal operation mode or that are safety critical must always be accessible in the vehicle.

It is well acknowledged that sharing information among different networked systems often results in overutilization of the available communication resources [26]. Due to the limited network bandwidth, data sampling and controller/estimator updates should be kept to the minimum required to ensure efficient use of the communication resources and to save network bandwidth. This idea has motivated the adoption of different event-triggered mechanisms (ETMs) to determine when data should be transmitted over the network [26]–[29].

Traditionally, the triggering mechanism is constructed based on when current measurement signals (or system states) have changed sufficiently in comparison with previous data such that a triggering condition is violated [30], [31]. Nevertheless, recent works have proved that, if the integral-based event condition is designed by integrating measurement signals (or system states) over a finite period, the amount of information sent through the network can be reduced in some applications [32], [33]. In [34], an integral-based event-triggered control that uses the integrals of system states to construct the event conditions is proposed. Numerical examples show that the requirements on the derivative of the Lyapunov function are relaxed, thus yielding improved sampling performance. These works focused on the design of controllers, but none of them considered parameter uncertainties. Li et al. [35] studied integral-based event-triggered fault estimation and impulsive fault-tolerant control for networked control systems. Although their work proposed an observer using an integral-based event-triggered mechanism, it did not consider parameter uncertainties, nor the possibility of Zeno behavior [36].

Motivated by the discussion above, the main novelty of this paper is the design of an integral-based event-triggered H_∞ observer to simultaneously estimate the sideslip and roll angles, considering intravehicle communications with a networked-induced delay. Both parameter uncertainties and disturbances are considered when designing the observer. Moreover, a positive lower bound on interevent times in the event-triggered observer is provided to eliminate Zeno behavior. Based on an augmented Lyapunov–Krasovskii functional, sufficient conditions on the design of the integral-based event-triggered parameters and the observer to achieve global asymptotic stability are established in terms of linear matrix inequalities (LMIs). A comparison of the proposed observer with results previously presented by the authors [37], where a traditional event-triggering mechanism is used, shows that the number of measurements that need to be transmitted decreases while the estimates for both angles are very similar. The simulation and experimental results demonstrate the effectiveness of the proposed observer.

Notation: Standard notation is used throughout this paper: $\mathbb{R}^n$ denotes an n-dimensional real vector space. $\mathbb{R}^{m\times n}$ denote real matrices with dimensions of $m \times n$. A superscript "T" represents the transpose of a matrix, while "**I**" and "**0**" denote identity and zero matrices of appropriate dimensions, respectively. The word "$diag$" stands for diagonal matrix. The symbol "$*$" denotes the symmetric term in a symmetric matrix.

II. Preliminaries and Problem Formulation

When driving a vehicle, both its longitudinal velocity, v_x, and the cornering stiffnesses of the front/rear tires, $C_{\alpha f}$ and $C_{\alpha r}$, can vary significantly. As both parameters have a strong influence on the lateral stability of the vehicle [19], [38], [39], these time-varying parameter uncertainties must be considered in the design of the observer. It is assumed that the velocity is measurable online in a polytope space. On the other hand, when the vehicle is running, the tire lateral stiffnesses vary but their values are unknown. In this case, these parameters can be represented by their nominal values and the bounds of their variations ($C_{\alpha f} + \Delta C_{\alpha f}$ and $C_{\alpha r} + \Delta C_{\alpha r}$).

The framework of the integral-based event-triggered H_∞ observer system is depicted in Figure 1. According to this, the observer is situated far from the sensors and the data are transmitted in a single packet over the communication network, which suffers from time delays. The data provided by the sensors are the steering wheel angle, $\delta(t)$, the longitudinal velocity, $v_x(t)$, the yaw rate, $r(t)$, and the roll rate, $\dot{\phi}(t)$. Assuming that the sensors' signals are measured with a sampling period h, the sampled signals are encapsulated into a data packet, $\{\delta(ih),\, v_x(ih),\, \mathbf{y}(ih) = [r(ih),\, \dot{\phi}(ih)]^T\}$ ($i = 1, 2, \ldots$), and sent to the integral-based event trigger (IET) module that determines when to transmit the information to the proposed observer over the communication network. Under the event-triggered condition, the data packets are released at instants $i_k h$ ($k = 1, 2, \ldots$).

The communication network induces a time delay η_k at the kth triggering instant between the sensor and observer that satisfies $0 < \eta_m \leq \eta_k \leq \eta_M$, where η_m and η_M are the lower and upper bound on the transmission delay, respectively. The lower bound is defined to avoid Zeno behavior [40].

Finally, the data are kept unchanged via a zero-order hold (ZOH) until the observer receives the next data packet from the network, to transform the discrete-time data into continuous-time information $\{\check{\delta}(t), \check{v}_x(t), \check{\mathbf{y}}(t)\}$.

A. Mathematical Vehicle Modeling

For the design of the observer, only the lateral vehicle dynamics is considered, so the influence of the pitch angle is ignored. The more complex the vehicle model, the more

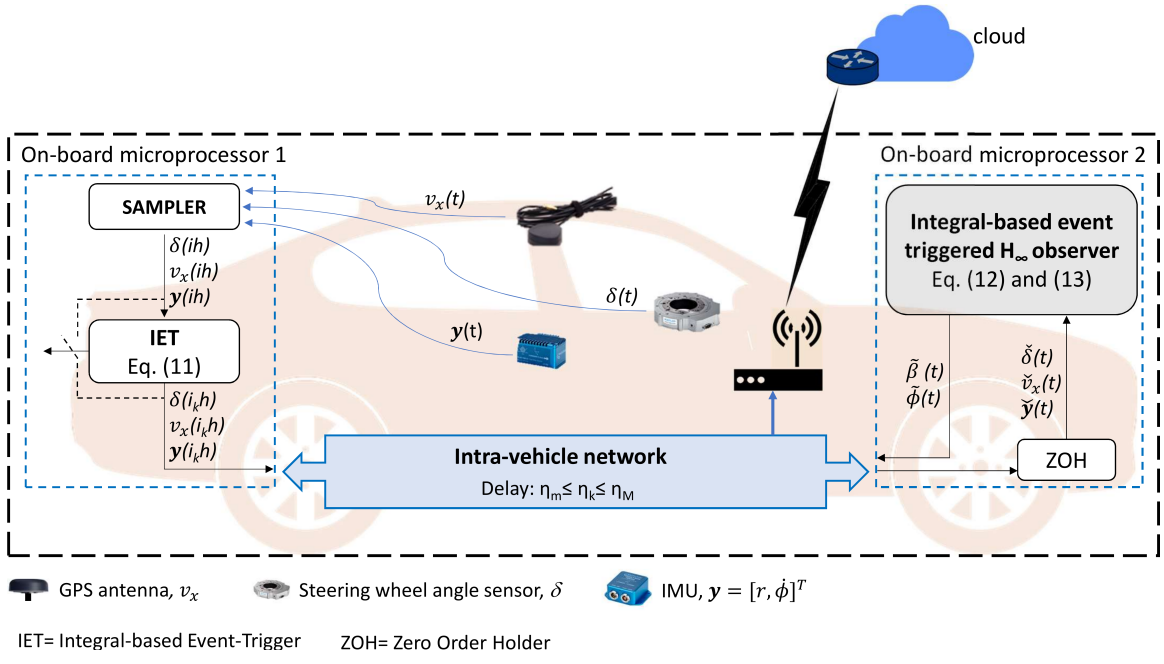

Fig. 1. Scheme of the networked system with the proposed integral-based event-triggered H_∞ observer

restrictive the problem to be solved. We adopt a model of the vehicle's lateral dynamics that includes lateral, roll, and yaw motions around the center of mass. The equivalent first-order state-space model of the vehicle is given as [37], [41]

$$\dot{\mathbf{x}}(t) = (\mathbf{A}(\rho) + \Delta\mathbf{A}(\rho))\,\mathbf{x}(t) + (\mathbf{B}_\delta(\rho) + \Delta\mathbf{B}_\delta(\rho))\,\check{\delta}(t) + (\mathbf{B}_u(\rho) + \Delta\mathbf{B}_u(\rho))\,\mathbf{u}(t) + \mathbf{B}_w(\rho)\,\mathbf{w}(t), \quad (1)$$

$$\mathbf{y}(t) = \mathbf{C}\mathbf{x}(t), \quad (2)$$

where $\mathbf{x} = \begin{bmatrix} \beta & r & \phi & \dot{\phi} \end{bmatrix}^T$ is the state vector given by the sideslip angle, β, yaw rate, r, roll angle, ϕ, and roll rate, $\dot{\phi}$; δ is the wheel steering angle; $\mathbf{y} = \begin{bmatrix} r & \dot{\phi} \end{bmatrix}^T$ is the measured output vector; $\mathbf{u} = \begin{bmatrix} \delta_c & M_\phi \end{bmatrix}^T$ is the control input vector given by the commanded steer angle δ_c and the corrective yaw moment M_ϕ and $\mathbf{w} = \begin{bmatrix} \phi_r & \dot{p}_f & d \end{bmatrix}^T$ is the disturbance vector given by the road bank angle ϕ_r, the x component of the angular velocity vector of the vehicle frame with respect to the inertial coordinates, $\dot{p}_f$, and d is the system noise. In this work, the vehicle is not controlled, so that $\mathbf{u} = \mathbf{0}$. By considering the control matrix, $\mathbf{B_u}$, a controller can be added to the vehicle architecture in the future, without having to modify the designed observer. Δ denotes the unknown uncertainties in the model. The nominal and uncertain matrices are continuous functions that depend on the time-varying parameter vector $\rho = [1/v_x \;\; 1/v_x^2]^T$ whose measurement is available in real time:

$$\mathbf{A}(\rho) = \begin{bmatrix} -\frac{I_{eq}C_0}{I_x m v_x} & -\left(1 + \frac{I_{eq}C_1}{I_x m v_x^2}\right) & \frac{h(mgh_{cr} - K_\phi)}{I_x v_x} & -\frac{h_{cr}C_\phi}{I_x v_x} \\ -\frac{C_1}{I_z} & -\frac{C_2}{I_z v_x} & 0 & 0 \\ 0 & 0 & 0 & 1 \\ -\frac{C_0 h_{cr}}{I_x} & -\frac{C_1 h_{cr}}{I_x v_x} & \frac{(mgh_{cr} - K_\phi)}{I_x} & -\frac{C_\phi}{I_x} \end{bmatrix},$$

$$\mathbf{B}_\delta(\rho) = \begin{bmatrix} \frac{I_{eq}C_{\alpha f}}{I_x m v_x} \\ \frac{l_f C_{\alpha f}}{I_z} \\ 0 \\ \frac{C_{\alpha f} h_{cr}}{I_x} \end{bmatrix}, \; \mathbf{B}_u(\rho) = \begin{bmatrix} \frac{I_{eq}C_{\alpha f}}{I_x m v_x} & 0 \\ \frac{l_f C_{\alpha f}}{I_z} & 0 \\ 0 & 0 \\ \frac{C_{\alpha f} h_{cr}}{I_x} & \frac{1}{I_x} \end{bmatrix},$$

$$\mathbf{B}_w(\rho) = \begin{bmatrix} -\frac{g}{v_x} & 0 & 1 \\ 0 & 0 & 1 \\ 0 & 0 & 1 \\ 0 & -1 & 1 \end{bmatrix},$$

$$\Delta\mathbf{A}(\rho) = \begin{bmatrix} -\frac{I_{eq}\Delta C_0}{I_x m v_x} & -\frac{I_{eq}\Delta C_1}{I_x m v_x^2} & 0 & 0 \\ -\frac{\Delta C_1}{I_z} & -\frac{\Delta C_2}{I_z v_x} & 0 & 0 \\ 0 & 0 & 0 & 0 \\ -\frac{\Delta C_0 h_{cr}}{I_x} & -\frac{\Delta C_1 h_{cr}}{I_x v_x} & 0 & 0 \end{bmatrix},$$

$$\Delta\mathbf{B}_\delta(\rho) = \begin{bmatrix} \frac{I_{eq}\Delta C_{\alpha f}}{I_x m v_x} \\ \frac{a\Delta C_{\alpha f}}{I_z} \\ 0 \\ \frac{\Delta C_{\alpha f} h_{cr}}{I_x} \end{bmatrix}, \; \Delta\mathbf{B}_u(\rho) = \begin{bmatrix} \frac{I_{eq}\Delta C_{\alpha f}}{I_x m v_x} & 0 \\ \frac{a\Delta C_{\alpha f}}{I_z} & 0 \\ 0 & 0 \\ \frac{\Delta C_{\alpha f} h_{cr}}{I_x} & 0 \end{bmatrix},$$

where $C_0 = C_{\alpha f} + C_{\alpha r}$, $C_1 = l_f C_{\alpha f} - l_r C_{\alpha r}$, $C_2 = l_f^2 C_{\alpha f} + l_r^2 C_{\alpha r}$, $I_{eq} = I_x + m h_{cr}^2$, $\Delta C_0 = \Delta C_{\alpha f} + \Delta C_{\alpha r}$, $\Delta C_1 = l_f \Delta C_{\alpha f} - l_r \Delta C_{\alpha r}$, and $\Delta C_2 = l_f^2 \Delta C_{\alpha f} + l_r^2 \Delta C_{\alpha r}$. The uncertain matrices $\Delta\mathbf{A}(\rho)$, $\Delta\mathbf{B}_\delta(\rho)$, and $\Delta\mathbf{B}_u(\rho)$ are assumed to be bounded, with known bounds

$$\begin{cases} -\mathbf{E}_A(\rho) \le \Delta\mathbf{A}(\rho) \le \mathbf{E}_A(\rho), \\ -\mathbf{E}_{\mathbf{B}_\delta}(\rho) \le \Delta\mathbf{B}_\delta(\rho) \le \mathbf{E}_{\mathbf{B}_\delta}(\rho), \\ -\mathbf{E}_{\mathbf{B}_u}(\rho) \le \Delta\mathbf{B}_u(\rho) \le \mathbf{E}_{\mathbf{B}_u}(\rho). \end{cases} \quad (3)$$

In this case, the uncertain matrices can be modeled as

$$\begin{cases} \Delta\mathbf{A}(\rho) = \mathbf{E}_A(\rho)\mathbf{M}_A\mathbf{F}_A, \\ \Delta\mathbf{B}_\delta(\rho) = \mathbf{E}_{\mathbf{B}_\delta}(\rho)\mathbf{M}_{\mathbf{B}_\delta}\mathbf{F}_{\mathbf{B}_\delta}, \\ \Delta\mathbf{B}_u(\rho) = \mathbf{E}_{\mathbf{B}_u}(\rho)\mathbf{M}_{\mathbf{B}_u}\mathbf{F}_{\mathbf{B}_u}, \end{cases} \quad (4)$$

with $\mathbf{M}_\bullet$ being the matrix-valued uncertainty satisfying $\mathbf{M}_\bullet^T\mathbf{M}_\bullet \leq \mathbf{I}$ and $\mathbf{F}_\bullet$ being the identity matrices of appropriate dimensions.

Assuming that the longitudinal velocity v_x can vary in the range $[\underline{v}_x, \overline{v}_x]$, the time-varying parameter vector ρ can be represented as a combination of the N vertices ω_i of a convex polytope formed by two triangles with vertex ω_3 in common:

- First triangle
  - $\omega_1 = \left(\frac{1}{\overline{v}_x}, \frac{1}{\overline{v}_x^2}\right)$,
  - $\omega_2 = \left(\frac{(\overline{v}_x+3\underline{v}_x)}{4\overline{v}_x\underline{v}_x}, \frac{1}{2\overline{v}_x\underline{v}_x} + \frac{1}{2\overline{v}_x^2}\right)$,
  - $\omega_3 = \left(\frac{(\overline{v}_x+\underline{v}_x)}{2\overline{v}_x\underline{v}_x}, \frac{(\overline{v}_x+\underline{v}_x)^2}{4\overline{v}_x^2\underline{v}_x^2}\right)$.
- Second triangle
  - $\omega_3 = \left(\frac{(\overline{v}_x+\underline{v}_x)}{2\overline{v}_x\underline{v}_x}, \frac{(\overline{v}_x+\underline{v}_x)^2}{4\overline{v}_x^2\underline{v}_x^2}\right)$,
  - $\omega_4 = \left(\frac{(3\overline{v}_x+\underline{v}_x)}{4\overline{v}_x\underline{v}_x}, \frac{1}{2\overline{v}_x\underline{v}_x} + \frac{1}{2\underline{v}_x^2}\right)$,
  - $\omega_5 = \left(\frac{1}{\underline{v}_x}, \frac{1}{\underline{v}_x^2}\right)$.

For each of the two triangles, the polytopic representation is given by

$$\Xi = \sum_{i=1}^{N} \alpha_i \omega_i, \tag{5}$$

where $\sum_{i=1}^{N} \alpha_i(\rho) = 1$, $\alpha_i(\rho) \geq 0$, and $N = 3$.

We refer to [37], [42] for further details about the polytope. The model can then be redefined as

$$\dot{\mathbf{x}}(t) = \sum_{i=1}^{N} \alpha_i \Big[(\mathbf{A}_i + \Delta\mathbf{A}_i)\mathbf{x}(t) + (\mathbf{B}_{i,\delta} + \Delta\mathbf{B}_{i,\delta})\check{\delta}(t) + (\mathbf{B}_{i,u} + \Delta\mathbf{B}_{i,u})\mathbf{u}(t) + \mathbf{B}_{i,w}\mathbf{w}(t) \Big], \tag{6}$$

$$\mathbf{y}(t) = \mathbf{C}\mathbf{x}(t). \tag{7}$$

B. Integral-Based Event-Triggered Mechanism

As depicted in Figure 1, the data packet that contains the sampled sensor signals obtained with a constant sampling period h, $\{\delta(ih), v_x(ih), \mathbf{y}(ih)\}$ $(i = 1, 2, \ldots)$, is sent to the event generator, which determines whether the current data packet needs to be transmitted to the observer over the network. The release instant is denoted as $i_k h$, where $i_k \in \mathbb{N}$. Assuming that the last transmitted data packet is $\{\delta(i_k h), v_x(i_k h), \mathbf{y}(i_k h)\}$, the subsequently sampled data packet $\{\delta(i_k h + jh), v_x(i_k h + jh), \mathbf{y}(i_k h + jh)\}$ $(j = 0, 1, 2, \ldots)$, will be transmitted at instant $i_{k+1}h \triangleq i_k h + jh$ to the observer when the following integral-based event-triggering condition is satisfied [33]:

$$\epsilon^2 \int_{h-h_M}^{h} \mathbf{y}^T(i_k s + js)\Omega\mathbf{y}(i_k s + js)ds \leq \int_{h-h_M}^{h} \mathbf{e}_y(i_k s)^T\Omega\mathbf{e}_y(i_k s)ds, \tag{8}$$

where $\epsilon > 0$ is a threshold, $\Omega > 0$ is a weighting matrix, h_M is the maximum time between two successive triggering instants, and $\mathbf{e}_y(i_k h) = \mathbf{y}(i_k h) - \mathbf{y}(i_k h + jh)$ is the error between the current measured output vector and the last transmitted one. In this research, the value of h_M has been selected by trial and error, considering two aspects: (1) to obtain a feasible solution from Theorem 1 and (2) to obtain good performance in the estimation of both the sideslip and roll angles while achieving a reduction in the data transmission.

The integral-based event triggering mechanism consists of a comparison between the accumulated measurements and the accumulated difference of the observation vector between two successive triggering instants. This performs better from the data transmission reduction viewpoint when compared with the corresponding traditional event-triggered mechanism.

Assuming that the time delay induced by the communication network is η_k at release instant $i_k h$, the transmitted data packet $\{\delta(i_k h), v_x(i_k h), \mathbf{y}(i_k h)\}$ arrives at the ZOH module at instant $t_k = i_k h + \eta_k$. If data dropouts and disorders are supposed not to occur, the data packet received by the observer from the plant through the network is defined as $\{\check{\delta}(t), \check{v}_x(t), \check{\mathbf{y}}(t)\} = \{\delta(i_k h), v_x(i_k h), \mathbf{y}(i_k h)\}$ for $t \in [i_k h + \eta_k, i_{k+1}h + \eta_{k+1})$. η_k and η_{k+1} are the network delay of the latest and next ZOH arrival data packet, respectively.

According to [43], the holding time at ZOH is defined as

$$\eta(t) \triangleq t - i_k h, \quad t \in [i_k h + \eta_k, i_{k+1}h + \eta_{k+1}), \tag{9}$$

and the updated measured output vector, $\check{\mathbf{y}}(t)$, received by the observer can be rewritten as

$$\check{\mathbf{y}}(t) = \mathbf{e}_y(t) + \mathbf{y}(t - \eta(t)), \tag{10}$$

where the delay $\eta(t)$ satisfies $\eta_m \leq \eta_k \leq \eta(t) < \eta_k + h \leq \eta_M + h$.

Substituting $\mathbf{y}(t)$ and $\check{\mathbf{y}}(t)$ given by (2) and (10), respectively, into (8), one obtains

$$\epsilon^2 \int_{t-h_M}^{t} \Big(\mathbf{e}_y(s) + \mathbf{C}\mathbf{x}(s-\eta)\Big)^T \Omega \times \Big(\mathbf{e}_y(s) + \mathbf{C}\mathbf{x}(s-\eta)\Big)ds - \int_{t-h_M}^{t} \mathbf{e}_y^T(s)\Omega\mathbf{e}_y(s)ds \leq 0. \tag{11}$$

A demonstration that the integral-based event triggering mechanism ensures the existence of a minimum inter-event time for the closed-loop system can be found in [44] and [45].

III. Integral-Based Event-Triggered Observer Design

In this section,the integral-based event-triggered observer is designed as follows:

$$\dot{\tilde{\mathbf{x}}}(t) = \sum_{i=1}^{N} \alpha_i \Big[\mathbf{A}_i\tilde{\mathbf{x}}(t) + \mathbf{B}_{i,\delta}\check{\delta}(t) + \mathbf{B}_{i,u}\mathbf{u}(t) + \mathbf{L}_i\big(\check{\mathbf{y}}(t) - \tilde{\mathbf{y}}(t)\big) \Big], \tag{12}$$

$$\tilde{\mathbf{y}}(t) = \mathbf{C}\tilde{\mathbf{x}}(t), \tag{13}$$

where L_i are the observation gain matrices. Considering (10), the observer can be formulated as

$$\dot{\tilde{\mathbf{x}}}(t) = \sum_{i=1}^{N} \alpha_i \Big[\mathbf{A}_i \tilde{\mathbf{x}}(t) + \mathbf{B}_{i,\delta} \check{\delta}(t) + \mathbf{B}_{i,u} \mathbf{u}(t) + \mathbf{L}_i \big(\mathbf{e}_y(t) + \mathbf{C}\big(\mathbf{x}(t-\eta(t)) - \tilde{\mathbf{x}}(t) \big) \big) \Big], \quad (14)$$

$$\tilde{\mathbf{y}}(t) = \mathbf{C}\tilde{\mathbf{x}}(t). \quad (15)$$

Defining $\mathbf{e}_x(t) = \mathbf{x}(t) - \tilde{\mathbf{x}}(t)$ as the state estimation error and combining (6) and (14), the error dynamics can be obtained as

$$\begin{aligned} \dot{\mathbf{e}}_x(t) &= \dot{\mathbf{x}}(t) - \dot{\tilde{\mathbf{x}}}(t) \\ &= \sum_{i=1}^{N} \alpha_i \Big[\mathbf{A}_i \big(\mathbf{x}(t) - \tilde{\mathbf{x}}(t) \big) - \mathbf{L}_i \mathbf{C} \mathbf{e}_x(t) + \Delta\mathbf{A}_i \mathbf{x}(t) \\ &\quad + \Delta\mathbf{B}_{i,\delta} \check{\delta}(t) + \Delta\mathbf{B}_{i,u} \mathbf{u}(t) + \mathbf{B}_{i,w} \mathbf{w}(t) \\ &\quad - \mathbf{L}_i \big(\mathbf{e}_y(t) + \mathbf{C}\big(\mathbf{x}(t-\eta(t)) - \mathbf{x}(t) \big) \big) \Big]. \end{aligned} \quad (16)$$

If we define an augmented state vector as $\xi(t) = \begin{bmatrix} \mathbf{e}_x(t) & \mathbf{x}(t) \end{bmatrix}^T$, (14) and (16) are transformed into the following augmented form:

$$\dot{\xi}(t) = \sum_{i=1}^{N} \alpha_i \Big[\left(\mathbf{A}_{0,i} + \Delta\mathbf{A}_{0,i} \right) \xi(t) + \mathbf{A}_{1,i} \xi(t-\eta(t)) + \mathbf{A}_{2,i} \mathbf{e}_y(t) + \left(\mathbf{A}_{3,i} + \Delta\mathbf{A}_{3,i} \right) \mathbf{q}(t) \Big], \quad (17)$$

where $\mathbf{q}(t) = \begin{bmatrix} \check{\delta}(t) & \mathbf{u}(t) & \mathbf{w}(t) \end{bmatrix}^T$ and

$$\mathbf{A}_{0,i} = \begin{bmatrix} (\mathbf{A}_i - \mathbf{L}_i\mathbf{C}) & \mathbf{L}_i\mathbf{C} \\ \mathbf{0} & \mathbf{A}_i \end{bmatrix}, \mathbf{A}_{1,i} = \begin{bmatrix} \mathbf{0} & \mathbf{L}_i\mathbf{C} \\ \mathbf{0} & \mathbf{0} \end{bmatrix},$$

$$\mathbf{A}_{2,i} = \begin{bmatrix} -\mathbf{L}_i \\ \mathbf{0} \end{bmatrix}, \mathbf{A}_{3,i} = \begin{bmatrix} \mathbf{0} & \mathbf{0} & \mathbf{B}_{w,i} \\ \mathbf{B}_{\delta,i} & \mathbf{B}_{u,i} & \mathbf{B}_{w,i} \end{bmatrix},$$

$$\Delta\mathbf{A}_{0,i} = \begin{bmatrix} \mathbf{0} & \Delta\mathbf{A}_i \\ \mathbf{0} & \Delta\mathbf{A}_i \end{bmatrix} = \bar{\mathbf{E}}_{A,i} \bar{\mathbf{M}}_A \bar{\mathbf{F}}_A,$$

$$\Delta\mathbf{A}_{3,i} = \begin{bmatrix} \Delta\mathbf{B}_{\delta,i} & \Delta\mathbf{B}_{u,i} & \mathbf{0} \\ \Delta\mathbf{B}_{\delta,i} & \Delta\mathbf{B}_{u,i} & \mathbf{0} \end{bmatrix} = \bar{\mathbf{E}}_{B,i} \bar{\mathbf{M}}_B \bar{\mathbf{F}}_B,$$

with

$$\bar{\mathbf{E}}_{A,i} = \begin{bmatrix} \mathbf{0} & \mathbf{E}_{A,i} \\ \mathbf{0} & \mathbf{E}_{A,i} \end{bmatrix}, \bar{\mathbf{M}}_A = \begin{bmatrix} \mathbf{M}_A & \mathbf{0} \\ \mathbf{0} & \mathbf{M}_A \end{bmatrix}, \bar{\mathbf{F}}_A = \begin{bmatrix} \mathbf{F}_A & \mathbf{0} \\ \mathbf{0} & \mathbf{F}_A \end{bmatrix},$$

$$\bar{\mathbf{E}}_B = \begin{bmatrix} \mathbf{E}_{B_\delta} & \mathbf{E}_{B_u} & \mathbf{0} \\ \mathbf{E}_{B_\delta} & \mathbf{E}_{B_u} & \mathbf{0} \end{bmatrix}, \bar{\mathbf{M}}_B = \begin{bmatrix} \mathbf{M}_{B_\delta} & \mathbf{0} & \mathbf{0} \\ \mathbf{0} & \mathbf{M}_{B_u} & \mathbf{0} \\ \mathbf{0} & \mathbf{0} & \mathbf{0} \end{bmatrix},$$

$$\bar{\mathbf{F}}_B = \begin{bmatrix} \mathbf{F}_{B_\delta} & \mathbf{0} & \mathbf{0} \\ \mathbf{0} & \mathbf{F}_{B_u} & \mathbf{0} \\ \mathbf{0} & \mathbf{0} & \mathbf{0} \end{bmatrix}.$$

For the theoretical development presented in later sections, the following definitions and lemmas are introduced:

Definition 1. *Given a scalar $\gamma > 0$, the system (17) is said to be asymptotically stable with an H_∞ performance index γ if, under zero initial conditions, the following inequality holds:*

$$\left\| \mathbf{z}^T(t)\mathbf{z}(t) \right\|_2 < \gamma \left\| \mathbf{q}^T(t)\mathbf{q}(t) \right\|_2, \quad (18)$$

where $\mathbf{z}(t) = \mathbf{C}_1 \xi(t)$ is the performance output and $\mathbf{C}_1 = \begin{bmatrix} \mathbf{I} & \mathbf{0} \end{bmatrix}$.

Lemma 1. *(Jensen's inequality). For any positive constant matrix $\mathbf{F} > 0 \in \mathbb{R}^{nxn}$, scalars $0 \le p_1 \le p_2$, and a vector function $\omega : [p_1, p_2] \to \mathbb{R}^n$ that is continuously differentiable, the following inequality holds:*

$$-\int_{p_1}^{p_2} \omega^T(s)\mathbf{F}\omega(s)ds \le -\frac{1}{p_2 - p_1} \left(\int_{p_1}^{p_2} \omega(s)ds \right)^T \mathbf{F} \left(\int_{p_1}^{p_2} \omega(s)ds \right).$$

Lemma 2. *[43] For any constant matrix $\mathbf{F} = \mathbf{F}^T \in \mathbb{R}^{nxn}$, matrix $\mathbf{T} \in \mathbb{R}^{nxn}$, scalars $0 < \tau_1 \le \tau(t) \le \tau_2$,and vector function $\omega : [-\tau_2, -\tau_1] \to \mathbb{R}^n$ such that the following integration is well defined, it holds that*

$$\begin{aligned} &-(\tau_2 - \tau_1) \int_{t-\tau_2}^{t-\tau_1} \dot{\omega}^T(s)\mathbf{F}\dot{\omega}(s)ds \\ &\le -\left(\omega(t-\tau_1) - \omega(t-\tau(t))\right)^T \mathbf{F} \left(\omega(t-\tau_1) - \omega(t-\tau(t))\right) \\ &\quad - \left(\omega(t-\tau(t)) - \omega(t-\tau_2)\right)^T \mathbf{F} \left(\omega(t-\tau(t)) - \omega(t-\tau_2)\right) \\ &\quad + \left(\omega(t-\tau_1) - \omega(t-\tau(t))\right)^T \mathbf{T}^T \left(\omega(t-\tau(t)) - \omega(t-\tau_2)\right) \\ &\quad + \left(\omega(t-\tau(t)) - \omega(t-\tau_2)\right)^T \mathbf{T} \left(\omega(t-\tau_1) - \omega(t-\tau(t))\right), \end{aligned}$$

when

$$\begin{bmatrix} \mathbf{F} & \mathbf{T} \\ \mathbf{T}^T & \mathbf{F} \end{bmatrix} \ge 0.$$

Lemma 3. *[46] For any matrix $\mathbf{R} > 0$, matrix $\mathbf{X} = \mathbf{X}^T$, and constant ρ, it holds that*

$$-\mathbf{X}\mathbf{R}^{-1}\mathbf{X} \le \rho^2\mathbf{R} - 2\rho\mathbf{X}.$$

To analyze the stability for each of the two polytope triangles of the designed observer given in the form of (12) and (13), the following theorem is developed:

Theorem 1. *For given scalars $\eta_m > 0$, $\eta_M > \eta_m$, $h > 0$, $h_M > 0$, $\epsilon > 0$, $\rho_1 > 0$, $\rho_2 > 0$, and $\gamma > 0$, the system (17) is asymptotically stable with an H_∞ performance index γ under the integral-based event-triggering condition if there exist scalars $\mu_1 > 0$ and $\mu_2 > 0$, definite-positive symmetric matrices $\mathbf{P} = \mathbf{P}^T > \mathbf{0}$, $\mathbf{Q}_{1,i} = \mathbf{Q}_{1,i}^T > \mathbf{0}$, $\mathbf{Q}_{2,i} = \mathbf{Q}_{2,i}^T > \mathbf{0}$, $\mathbf{R}_1 = \mathbf{R}_1^T > \mathbf{0}$, $\mathbf{R}_2 = \mathbf{R}_2^T > \mathbf{0}$, $\mathbf{\Omega} = \mathbf{\Omega}^T > 0$, and $\mathbf{Z} = \mathbf{Z}^T > \mathbf{0}$, and any matrices $\mathbf{S}$ and $\mathbf{M}_i$ of appropriate dimensions such that the following LMIs hold:*

$$\begin{bmatrix} \mathbf{\Gamma}_{11,i} & \mathbf{\Gamma}_{12,i} & \mathbf{\Gamma}_{13,i} & \mathbf{\Gamma}_{14,i} & \mathbf{\Gamma}_{15,i} \\ * & \mathbf{\Gamma}_{22,i} & \mathbf{0} & \mathbf{0} & \mathbf{0} \\ * & * & \mathbf{\Gamma}_{33,i} & \mathbf{\Gamma}_{34,i} & \mathbf{\Gamma}_{35,i} \\ * & * & * & -\mu_1\mathbf{I} & \mathbf{0} \\ * & * & * & * & -\mu_2\mathbf{I} \end{bmatrix} < \mathbf{0} \quad \text{for } i = 1, 2, \ldots, N, \quad (19)$$

$$\begin{bmatrix} \mathbf{R}_2 & \mathbf{S} \\ * & \mathbf{R}_2 \end{bmatrix} > \mathbf{0}, \quad (20)$$

with

$$\mathbf{\Gamma}_{11,i}=\begin{bmatrix}\mathbf{\Gamma}_{11}^{11,i} & \mathbf{\Gamma}_{12}^{11,i} & \mathbf{R} & \mathbf{0} & \mathbf{\Gamma}_{15}^{11,i} & \mathbf{\Gamma}_{16}^{11,i}\\ * & \mathbf{\Gamma}_{22}^{11,i} & \mathbf{\Gamma}_{23}^{11,i} & \mathbf{\Gamma}_{24}^{11,i} & \mathbf{0} & \mathbf{0}\\ * & * & \mathbf{\Gamma}_{33}^{11,i} & \mathbf{\Gamma}_{34}^{11,i} & \mathbf{0} & \mathbf{0}\\ * & * & * & \mathbf{\Gamma}_{44}^{11,i} & \mathbf{0} & \mathbf{0}\\ * & * & * & * & -\mathbf{Z} & \mathbf{0}\\ * & * & * & * & * & -\gamma^2\mathbf{I}\end{bmatrix},$$

$$\mathbf{\Gamma}_{11}^{11,i}=\begin{bmatrix}\Delta_{11,i} & \mathbf{M}_i\mathbf{C}+\mathbf{Q}_{112,i}-\mathbf{R}_{112}\\ * & \mathbf{P}_2\mathbf{A}_i+\mathbf{A}_i^T\mathbf{P}_2+\mathbf{Q}_{122}-\mathbf{R}_{122}\end{bmatrix},$$

$$\Delta_{11,i}=(\mathbf{P}_1\mathbf{A}_i-\mathbf{M}_i\mathbf{C})+(\mathbf{P}_1\mathbf{A}_i-\mathbf{M}_i\mathbf{C})^T+\mathbf{Q}_{111,i}-\mathbf{R}_{111},$$

$$\mathbf{\Gamma}_{12}^{11,i}=\begin{bmatrix}\mathbf{0} & -\mathbf{M}_i\mathbf{C}\\ \mathbf{0} & \mathbf{0}\end{bmatrix},\ \mathbf{\Gamma}_{15}^{11,i}=\begin{bmatrix}-\mathbf{M}_i\\ \mathbf{0}\end{bmatrix},$$

$$\mathbf{\Gamma}_{16}^{11,i}=\begin{bmatrix}\mathbf{0} & \mathbf{0} & \mathbf{P}_1\mathbf{B}_{w,i}\\ \mathbf{P}_2\mathbf{B}_{i,\delta} & \mathbf{P}_2\mathbf{B}_{i,u} & \mathbf{P}_2\mathbf{B}_{w,i}\end{bmatrix},$$

$$\mathbf{\Gamma}_{22}^{11,i}=-2\mathbf{R}_2-\mathbf{S}^T-\mathbf{S},\ \mathbf{\Gamma}_{23}^{11,i}=\mathbf{R}_2+\mathbf{S},$$

$$\mathbf{\Gamma}_{24}^{11,i}=\mathbf{R}_2+\mathbf{S}^T,\ \mathbf{\Gamma}_{33}^{11,i}=(\mathbf{Q}_{2,i}-\mathbf{Q}_{1,i})-\mathbf{R}_1-\mathbf{R}_2,$$

$$\mathbf{\Gamma}_{34}^{11,i}=-\mathbf{S}^T,\ \mathbf{\Gamma}_{44}^{11,i}=-\mathbf{Q}_{2,i}-\mathbf{R}_2,$$

$$\mathbf{\Gamma}_{12,i}=\begin{bmatrix}\mathbf{0}\ \mathbf{0}\ \mathbf{C}_1^T\\ \mathbf{0}\ \mathbf{0}\ \mathbf{0}\\ \mathbf{0}\ \mathbf{0}\ \mathbf{0}\\ \mathbf{0}\ \mathbf{0}\ \mathbf{0}\\ \mathbf{0}\ \mathbf{0}\ \mathbf{0}\\ \mathbf{0}\ \mathbf{0}\ \mathbf{0}\end{bmatrix},$$

$$\mathbf{\Gamma}_{13,i}=\begin{bmatrix}\mathbf{\Gamma}_{11}^{13,i} & \mathbf{\Gamma}_{12}^{13,i} & \mathbf{\Gamma}_{13}^{13,i} & \mathbf{\Gamma}_{14}^{13,i}\\ \mathbf{\Gamma}_{21}^{13,i} & \mathbf{\Gamma}_{22}^{13,i} & \mathbf{\Gamma}_{23}^{13,i} & \mathbf{\Gamma}_{24}^{13,i}\\ \mathbf{0} & \mathbf{0} & \mathbf{0} & \mathbf{0}\\ \mathbf{0} & \mathbf{0} & \mathbf{0} & \mathbf{0}\\ -\eta_m\mathbf{M}_i^T & \mathbf{0} & -(\bar{\eta}-\eta_m)\mathbf{M}_i^T & \mathbf{0}\\ \mathbf{\Gamma}_{61}^{13,i} & \mathbf{\Gamma}_{62}^{13,i} & \mathbf{\Gamma}_{63}^{13,i} & \mathbf{\Gamma}_{64}^{13,i}\end{bmatrix},$$

$$\mathbf{\Gamma}_{11}^{13,i}=\begin{bmatrix}\eta_m\left(\mathbf{A}_i^T\mathbf{P}_1-\mathbf{C}^T\mathbf{M}_i^T\right)\\ \eta_m\mathbf{C}^T\mathbf{M}_i^T\end{bmatrix},\ \mathbf{\Gamma}_{12}^{13,i}=\begin{bmatrix}\mathbf{0}\\ \eta_m\mathbf{A}_i^T\mathbf{P}_2\end{bmatrix},$$

$$\mathbf{\Gamma}_{13}^{13,i}=\begin{bmatrix}(\bar{\eta}-\eta_m)\left(\mathbf{A}_i^T\mathbf{P}_1-\mathbf{C}^T\mathbf{M}_i^T\right)\\ (\bar{\eta}-\eta_m)\mathbf{C}^T\mathbf{M}_i^T\end{bmatrix},$$

$$\mathbf{\Gamma}_{14}^{13,i}=\begin{bmatrix}\mathbf{0}\\ (\bar{\eta}-\eta_m)\mathbf{A}_i^T\mathbf{P}_2\end{bmatrix},\ \mathbf{\Gamma}_{21}^{13,i}=\begin{bmatrix}\mathbf{0}\\ -\eta_m\mathbf{C}^T\mathbf{M}_i^T\end{bmatrix},$$

$$\mathbf{\Gamma}_{22}^{13,i}=\mathbf{\Gamma}_{24}^{13,i}=\begin{bmatrix}\mathbf{0}\\ \mathbf{0}\end{bmatrix},\ \mathbf{\Gamma}_{23}^{13,i}=\begin{bmatrix}\mathbf{0}\\ -(\bar{\eta}-\eta_m)\mathbf{C}^T\mathbf{M}_i^T\end{bmatrix},$$

$$\mathbf{\Gamma}_{61}^{13,i}=\begin{bmatrix}\mathbf{0}\\ \mathbf{0}\\ \eta_m\mathbf{B}_{w,i}^T\mathbf{P}_1\end{bmatrix},\ \mathbf{\Gamma}_{62}^{13,i}=\begin{bmatrix}\eta_m\mathbf{B}_{i,\delta}^T\mathbf{P}_2\\ \eta_m\mathbf{B}_{i,u}^T\mathbf{P}_2\\ \eta_m\mathbf{B}_{w,i}^T\mathbf{P}_2\end{bmatrix},$$

$$\mathbf{\Gamma}_{63}^{13,i}=\begin{bmatrix}\mathbf{0}\\ \mathbf{0}\\ (\bar{\eta}-\eta_m)\mathbf{B}_{w,i}^T\mathbf{P}_1\end{bmatrix},$$

$$\mathbf{\Gamma}_{64}^{13,i}=\begin{bmatrix}(\bar{\eta}-\eta_m)\mathbf{B}_{i,\delta}^T\mathbf{P}_2\\ (\bar{\eta}-\eta_m)\mathbf{B}_{i,u}^T\mathbf{P}_2\\ (\bar{\eta}-\eta_m)\mathbf{B}_{w,i}^T\mathbf{P}_2\end{bmatrix},$$

$$\mathbf{\Gamma}_{14,i}=\begin{bmatrix}\mathbf{\Gamma}_{11}^{14,i} & \mathbf{\Gamma}_{12}^{14,i}\\ \mathbf{0} & \mathbf{0}\\ \mathbf{0} & \mathbf{0}\\ \mathbf{0} & \mathbf{0}\\ \mathbf{0} & \mathbf{0}\\ \mathbf{0} & \mathbf{0}\end{bmatrix},\ \mathbf{\Gamma}_{15,i}=\begin{bmatrix}\mathbf{\Gamma}_{11}^{15,i} & \mathbf{0}\\ \mathbf{0} & \mathbf{0}\\ \mathbf{0} & \mathbf{0}\\ \mathbf{0} & \mathbf{0}\\ \mathbf{0} & \mathbf{0}\\ \mathbf{0} & \mathbf{\Gamma}_{16}^{15,i}\end{bmatrix},$$

$$\mathbf{\Gamma}_{11}^{14,i}=\begin{bmatrix}\mathbf{0}\ \mathbf{P}_1\mathbf{E}_A\\ \mathbf{0}\ \mathbf{P}_2\mathbf{E}_A\end{bmatrix},\ \mathbf{\Gamma}_{12}^{14,i}=\begin{bmatrix}\mu_1\mathbf{F}_A^T & \mathbf{0}\\ \mathbf{0} & \mu_1\mathbf{F}_A^T\end{bmatrix},$$

$$\mathbf{\Gamma}_{11}^{15,i}=\begin{bmatrix}\mathbf{P}_1\mathbf{E}_{\mathbf{B}_\delta}\ \mathbf{P}_1\mathbf{E}_{\mathbf{B}_\delta}\ \mathbf{0}\\ \mathbf{P}_2\mathbf{E}_{\mathbf{B}_\delta}\ \mathbf{P}_2\mathbf{E}_{\mathbf{B}_u}\ \mathbf{0}\end{bmatrix},$$

$$\mathbf{\Gamma}_{16}^{15,i}=\begin{bmatrix}\mu_2\mathbf{F}_{\mathbf{B}_\delta}^T & \mathbf{0} & \mathbf{0}\\ \mathbf{0} & \mu_2\mathbf{F}_{\mathbf{B}_\delta}^T & \mathbf{0}\\ \mathbf{0} & \mathbf{0} & \mathbf{0}\end{bmatrix},$$

$$\mathbf{\Gamma}_{22,i}=\begin{bmatrix}\Theta^T\frac{\epsilon^2}{h_M}\Omega\Theta & \Theta^T\frac{\epsilon^2}{h_M}\Omega & \mathbf{0}\\ * & -\frac{\Omega}{h_M}+\frac{\epsilon^2}{h_M}\Omega & \mathbf{0}\\ * & * & -\mathbf{I}\end{bmatrix},$$

$$\mathbf{\Gamma}_{33,i}=\begin{bmatrix}\mathbf{\Gamma}_{11}^{33,i} & \mathbf{0}\\ * & \mathbf{\Gamma}_{22}^{33,i}\end{bmatrix},\ \mathbf{\Gamma}_{34,i}=\begin{bmatrix}\mathbf{\Gamma}_{11}^{34,i} & \mathbf{0}\\ \mathbf{\Gamma}_{21}^{34,i} & \mathbf{0}\end{bmatrix},$$

$$\mathbf{\Gamma}_{11}^{33,i}=\begin{bmatrix}\rho_1^2\mathbf{R}_{111}-2\rho_1\mathbf{P}_1 & \rho_1^2\mathbf{R}_{112}\\ * & \rho_1^2\mathbf{R}_{122}-2\rho_1\mathbf{P}_2\end{bmatrix},$$

$$\mathbf{\Gamma}_{22}^{33,i}=\begin{bmatrix}\rho_2^2\mathbf{R}_{211}-2\rho_2\mathbf{P}_1 & \rho_2^2\mathbf{R}_{212}\\ * & \rho_2^2\mathbf{R}_{222}-2\rho_2\mathbf{P}_2\end{bmatrix},$$

$$\mathbf{\Gamma}_{11}^{34,i}=\begin{bmatrix}\mathbf{0}\ \eta_m\mathbf{P}_1\mathbf{E}_A\\ \mathbf{0}\ \eta_m\mathbf{P}_2\mathbf{E}_A\end{bmatrix},\ \mathbf{\Gamma}_{21}^{34,i}=\begin{bmatrix}\mathbf{0}\ (\bar{\eta}-\eta_m)\mathbf{P}_1\mathbf{E}_A\\ \mathbf{0}\ (\bar{\eta}-\eta_m)\mathbf{P}_2\mathbf{E}_A\end{bmatrix},$$

$$\mathbf{\Gamma}_{35,i}=\begin{bmatrix}\mathbf{\Gamma}_{11}^{35,i}\ \mathbf{0}\\ \mathbf{\Gamma}_{21}^{35,i}\ \mathbf{0}\end{bmatrix},$$

$$\mathbf{\Gamma}_{11}^{35,i}=\begin{bmatrix}\eta_m\mathbf{P}_1\mathbf{E}_{\mathbf{B}_\delta}\ \eta_m\mathbf{P}_1\mathbf{E}_{\mathbf{B}_u}\ \mathbf{0}\\ \eta_m\mathbf{P}_2\mathbf{E}_{\mathbf{B}_\delta}\ \eta_m\mathbf{P}_2\mathbf{E}_{\mathbf{B}_u}\ \mathbf{0}\end{bmatrix},$$

$$\mathbf{\Gamma}_{21}^{35,i}=\begin{bmatrix}(\bar{\eta}-\eta_m)\mathbf{P}_1\mathbf{E}_{\mathbf{B}_\delta}\ (\bar{\eta}-\eta_m)\mathbf{P}_1\mathbf{E}_{\mathbf{B}_u}\ \mathbf{0}\\ (\bar{\eta}-\eta_m)\mathbf{P}_2\mathbf{E}_{\mathbf{B}_\delta}\ (\bar{\eta}-\eta_m)\mathbf{P}_2\mathbf{E}_{\mathbf{B}_u}\ \mathbf{0}\end{bmatrix},$$

with

$$\mathbf{P}=\begin{bmatrix}\mathbf{P}_1 & \mathbf{0}\\ \mathbf{0} & \mathbf{P}_2\end{bmatrix},\ \mathbf{S}=\begin{bmatrix}\mathbf{S}_{11} & \mathbf{S}_{12}\\ * & \mathbf{S}_{22}\end{bmatrix},$$

$$\mathbf{R}_1=\begin{bmatrix}\mathbf{R}_{111} & \mathbf{R}_{112}\\ * & \mathbf{R}_{122}\end{bmatrix},\ \mathbf{R}_2=\begin{bmatrix}\mathbf{R}_{211} & \mathbf{R}_{212}\\ * & \mathbf{R}_{222}\end{bmatrix},$$

$$\mathbf{Q}_{1,i}=\begin{bmatrix}\mathbf{Q}_{111,i} & \mathbf{Q}_{112,i}\\ * & \mathbf{Q}_{122,i}\end{bmatrix},\ \mathbf{Q}_{2,i}=\begin{bmatrix}\mathbf{Q}_{211,i} & \mathbf{Q}_{212,i}\\ * & \mathbf{Q}_{222,i}\end{bmatrix}.$$

Then, the observer gains $\mathbf{L}_i$ *are given by* $\mathbf{L}_i=\mathbf{P}_1^{-1}\mathbf{M}_i$.

Proof: See Appendix A. ■

TABLE I
LATERAL DYNAMICS MODEL PARAMETERS OF THE MERCEDES SPRINTER VAN

Description	Parameter	Value
Total vehicle mass	m	2150 kg
Distance from roll center to CoG	h_{cr}	0.35 m
Distance from CoG to front axle	l_f	1.51 m
Distance from CoG to rear axle	l_r	2.04 m
Front tire cornering stiffness	$C_{\alpha f}$	969.64 kN/rad
Rear tire cornering stiffness	$C_{\alpha r}$	1299.5 kN/rad
Roll moment of inertia	I_x	500 kg/m^2
Yaw moment of inertia	I_z	2975 kg/m^2
Roll stiffness	K_ϕ	53.825 kNm/rad
Roll damping coefficient	C_ϕ	5.448 kNms/rad

IV. RESULTS AND DISCUSSION

A. Simulation Results

In this subsection, the effectiveness of the proposed integral-based event-triggered H_∞ observer is tested on a simulated Mercedes Sprinter van model created in the software TruckSim® [47]. The parameters of the van's lateral dynamics model used for designing the observer are presented in Table I. For the simulation tests, it is assumed that the van's longitudinal velocity is bounded in the interval $[2\,\text{m/s}, 20\,\text{m/s}]$ and that the maximum variation of the front and rear tire cornering stiffnesses is 5% of their nominal values.

To perform the simulation tests, we recreated different driving maneuvers in the TruckSim® environment:

- Test 1: J-turn maneuver at 60 degrees of steering wheel steer angle and with a speed of 60 km/h on an asphalt road
- Test 2: double lane change at 70 km/h on an asphalt road
- Test 3: sine sweep maneuver for a frequency range from 0.05 to 0.5 Hz at 40 km/h on an asphalt road

These maneuvers are some of the most commonly used to analyze the handling, stability, and rollover propensity of a broad range of vehicles. During these maneuvers, the vehicle exhibits strongly nonlinear behavior. Each of the tests was carried out for three cases, considering different values of the sampling period h and minimum lower and maximum upper bounds η_m and η_M, respectively. h_M is defined to be equal to 50 s considering both that Theorem 1 has a feasible solution and vehicle safety. Both simulation and experimental results have shown that a value of h_M equal to 50 s is adequate. Table II presents the parameters used in the design of the proposed observer. The LMIs (19) and (20) in Theorem 1 were solved offline by using the LMI toolbox in MATLAB to obtain the observer gains, $\mathbf{L_i}$, and the triggering parameters, $\mathbf{\Omega_i}$, for the three cases:

- Case A
  - First triangle of the polytope

$$\Omega_1 = \begin{bmatrix} 185.222 & 0 \\ 0 & 185.222 \end{bmatrix}, \ \mathbf{L_1} = \begin{bmatrix} 0.368 & -0.444 \\ -4.389 & 4.582 \\ -0.164 & -0.109 \\ 3.817 & 1.883 \end{bmatrix},$$

$$\mathbf{L_2} = \begin{bmatrix} 0.516 & -0.244 \\ -12.884 & 6.811 \\ -0.020 & -0.157 \\ 3.361 & 2.339 \end{bmatrix}, \ \mathbf{L_3} = \begin{bmatrix} -1.605 & 1.578 \\ 16.480 & -19.303 \\ 0.014 & -0.192 \\ -6.454 & 10.541 \end{bmatrix}.$$

  - Second triangle of the polytope

$$\Omega_2 = \begin{bmatrix} 41.410 & 0 \\ 0 & 41.410 \end{bmatrix}, \ \mathbf{L_3} = \begin{bmatrix} 5.143 & -0.914 \\ -24.096 & 3.518 \\ -0.130 & -0.139 \\ 8.900 & 3.563 \end{bmatrix},$$

$$\mathbf{L_4} = \begin{bmatrix} -1.075 & -0.475 \\ 4.177 & 0.840 \\ -0.006 & -0.149 \\ -1.811 & 4.680 \end{bmatrix}, \ \mathbf{L_5} = \begin{bmatrix} -11.464 & 0.688 \\ 41.785 & -3.662 \\ 0.054 & -0.162 \\ -16.305 & 7.008 \end{bmatrix}.$$

- Case B
  - First triangle of the polytope

$$\Omega_1 = \begin{bmatrix} 183.697 & 0 \\ 0 & 183.697 \end{bmatrix}, \ \mathbf{L_1} = \begin{bmatrix} 0.330 & -0.446 \\ -3.994 & 4.441 \\ -0.1574 & -0.114 \\ 3.459 & 1.937 \end{bmatrix},$$

$$\mathbf{L_2} = \begin{bmatrix} 0.520 & -0.246 \\ -13.440 & 6.870 \\ -0.024 & -0.152 \\ 3.481 & 2.375 \end{bmatrix},$$

$$\mathbf{L_3} = \begin{bmatrix} -1.416 & 1.713 \\ 13.896 & -20.863 \\ -0.002 & -0.196 \\ -5.821 & 10.940 \end{bmatrix}.$$

  - Second triangle of the polytope

$$\Omega_2 = \begin{bmatrix} 48.151 & 0 \\ 0 & 48.151 \end{bmatrix}, \ \mathbf{L_3} = \begin{bmatrix} 4.708 & -0.936 \\ -23.060 & 3.504 \\ -0.128 & -0.143 \\ 8.341 & 3.679 \end{bmatrix},$$

$$\mathbf{L_4} = \begin{bmatrix} -1.070 & -0.481 \\ 4.162 & 0.826 \\ -0.006 & -0.153 \\ -1.834 & 4.852 \end{bmatrix}, \ \mathbf{L_5} = \begin{bmatrix} 4.708 & -0.936 \\ -23.060 & 3.504 \\ -0.128 & -0.143 \\ 8.341 & 3.679 \end{bmatrix}.$$

- Case C
  - First triangle of the polytope

$$\Omega_1 = \begin{bmatrix} 195.676 & 0 \\ 0 & 195.676 \end{bmatrix}, \ \mathbf{L_1} = \begin{bmatrix} 0.575 & -0.431 \\ -6.164 & 5.263 \\ -0.194 & -0.091 \\ 5.683 & 1.617 \end{bmatrix},$$

$$\mathbf{L_2} = \begin{bmatrix} 0.653 & -0.256 \\ -14.412 & 6.964 \\ -0.049 & -0.178 \\ 3.986 & 2.119 \end{bmatrix},$$

$$\mathbf{L_3} = \begin{bmatrix} -2.167 & 0.931 \\ 25.262 & -11.827 \\ 0.066 & -0.169 \\ -8.110 & 8.453 \end{bmatrix}.$$

– Second triangle of the polytope

$$\Omega_2 = \begin{bmatrix} 40.317 & 0 \\ 0 & 40.317 \end{bmatrix}, \mathbf{L_3} = \begin{bmatrix} 6.696 & -0.952 \\ -28.403 & 4.100 \\ -0.139 & -0.121 \\ 11.063 & 2.813 \end{bmatrix},$$

$$\mathbf{L_4} = \begin{bmatrix} -1.388 & -0.430 \\ 5.785 & 0.905 \\ -0.001 & -0.137 \\ -2.347 & 3.997 \end{bmatrix}, \mathbf{L_5} = \begin{bmatrix} -10.122 & 0.696 \\ 38.734 & -4.066 \\ 0.039 & -0.151 \\ -14.882 & 6.417 \end{bmatrix}.$$

TABLE II
DESIGN PARAMETERS OF THE OBSERVER

	Case A	Case B	Case C
h (ms)	15	10	10
h_M (s)	50	50	50
η_m (ms)	5	5	5
η_M (ms)	20	20	50
γ	1		
ϵ^2	0.01		
ρ_1	1		
ρ_2	1		

Simulation results obtained from the proposed integral-based event-triggered H_∞ observer were compared with those obtained by considering a traditional event-triggered mechanism as described in [37]. For the traditional event-triggered mechanism, the observer gains and triggering parameters are listed in Appendix B. Tables III–V present the root-mean-square (RMS) and maximum errors of the estimated sideslip and roll angles obtained for the different tests and cases. The values estimated by both event-triggered mechanisms are very similar with a difference of less than 1 degree. The results confirm that the integral-based event-triggered mechanism reduces the number of data transmitted over the network in comparison with the traditional event-triggered mechanism, by up to 12%. Figure 2 shows a time-based plot of the simulated and estimated sideslip and roll angles, and the release instants for test 3 and case A for the traditional and integral-based event-triggered mechanisms. A comparison of these results confirm that the proposed observer exhibits better performance.

B. Experimental Results

To verify the feasibility and good performance of the proposed algorithm, experiments were carried out on two vehicles with different characteristics: a Mercedes Sprinter van and a GOKA 650 (Figure 3). Both are ISVA (Research Institute of Vehicle Safety) Laboratory test vehicles. They are equipped with:

- A Racelogic's inertial measurement unit (IMU) IMU04, providing highly accurate measurements of pitch, roll, and yaw rate using three rate gyros, as well as x, y, z acceleration via three accelerometers with the following specifications: $\pm 450°/s$ angular rate range in each axis, $\pm 20g$ acceleration range in each axis, $0.00085°/s$ angular rate resolution, and $0.00004g$ acceleration resolution.
- A Racelogic's VBOX 3i dual antenna with antennas mounted $90°$ to the true heading of the vehicle with the following main specifications: 100 Hz GPS/GLONASS data logging, 1 cm distance resolution, 0.01 km/h velocity resolution, $< 0.2°$ sideslip angle (RMS) accuracy and $< 0.14°$ roll angle (RMS) accuracy.
- A Kistler Universal measurement steering wheel DTI sensor with the following specifications: ± 250 Nm steering moment range, $\pm 1,250°$ steering angle range, $\leq 2,000°/s$ steering speed and $0.015°$ steering angle resolution.

For the experimental tests, it is assumed that the longitudinal velocity is bounded in the interval [2 m/s, 20 m/s]. The

TABLE III
SIMULATION RESULTS FOR TEST 1

	Traditional Event Triggering		Integral-Based Event Triggering	
	Sideslip Angle (deg)			
Case	RMS Error	Max. Error	RMS Error	Max. Error
A	0.91	1.63	0.88	1.60
B	0.90	1.59	0.90	1.64
C	0.90	1.55	0.89	1.61
	Roll Angle (deg)			
Case	RMS Error	Max. Error	RMS Error	Max.
A	0.50	0.80	0.57	0.70
B	0.47	0.85	0.54	0.79
C	0.47	0.91	0.58	1.00
Case	Non-transmission Rate (%)			
A	97.45		97.90	
B	98.10		98.30	
C	98.10		98.30	

TABLE IV
SIMULATION RESULTS FOR TEST 2

	Traditional Event Triggering		Integral-Based Event Triggering	
	Sideslip Angle (deg)			
Case	RMS Error	Max. Error	RMS Error	Max. Error
A	0.56	1.42	0.56	1.42
B	0.57	1.43	0.56	1.43
C	0.56	1.39	0.55	1.40
	Roll Angle (deg)			
Case	RMS Error	Max. Error	RMS Error	Max. Error
A	0.86	2.09	0.89	0.89
B	0.58	1.43	0.89	2.14
C	0.54	1.33	0.96	2.27
Case	Non-transmission Rate (%)			
A	51.87		57.87	
B	58.84		66.23	
C	58.84		66.23	

TABLE V
SIMULATION RESULTS FOR TEST 3

	Traditional Event Triggering		Integral-Based Event Triggering	
	Sideslip Angle (deg)			
Case	RMS Error	Max.	RMS Error	Max.
A	0.12	0.25	0.13	0.41
B	0.13	0.27	0.13	0.53
C	0.12	0.27	0.13	0.13
	Roll Angle (deg)			
Case	RMS Error	Max. Error	RMS Error	Max. Error
A	0.33	0.87	0.34	0.97
B	0.28	0.69	0.34	0.94
C	0.26	0.65	0.36	0.99
Case	Non-transmission Rate (%)			
A	75.93		80.53	
B	81.38		87.00	
C	81.39		87.00	

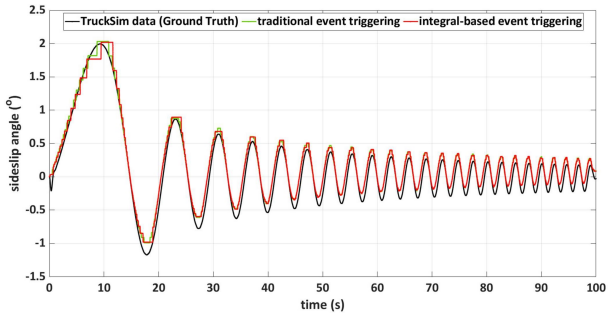

(a) Sideslip angle

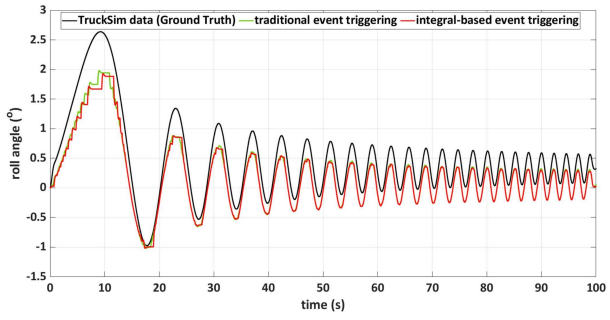

(b) Roll angle

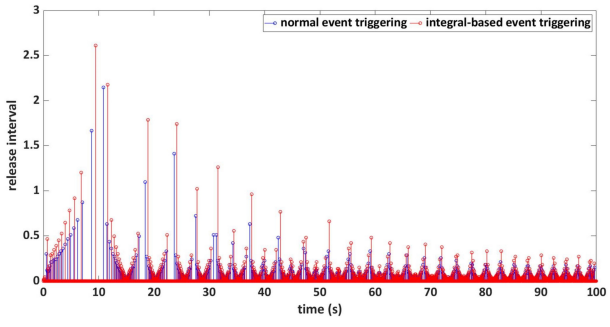

(c) Release instants

Fig. 2. Mercedes Sprinter van: simulation results for test 3 and case A

(a) Mercedes Sprinter van

(b) GOKA 650

Fig. 3. Test vehicles

maximum variation of the tire cornering stiffnesses is 5% and 1% of their nominal values, for the Mercedes Sprinter van and the GOKA 650, respectively. Concerning the GOKA 650, only case B is carried out.

Figures 4a and 5a show the maneuvers conducted with the Mercedes Sprinter van and the GOKA 650, respectively. The longitudinal velocity profiles corresponding to these maneuvers are depicted in Figures 4b and 5b. During the tests, the vehicles perform lane changes and turns on roundabouts.

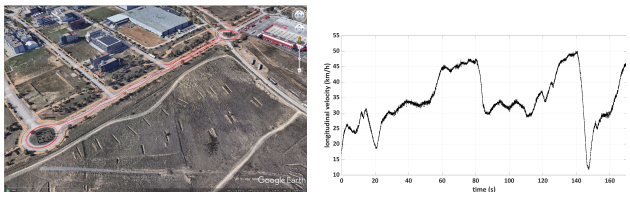

(a) Vehicle trajectory (b) Longitudinal speed

Fig. 4. Mercedes Sprinter van: vehicle trajectory and longitudinal speed for real maneuver

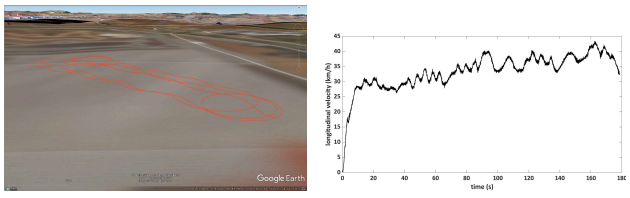

(a) Vehicle trajectory (b) Longitudinal speed

Fig. 5. GOKA 650: vehicle trajectory and longitudinal speed for real maneuver

TABLE VI
EXPERIMENTAL RESULTS FOR THE MERCEDES SPRINTER VAN

	Traditional Event Triggering		Integral-Based Event Triggering	
	Sideslip Angle (deg)			
Case	**RMS Error**	**Max. Error**	**RMS Error**	**Max. Error**
A	0.83	3.49	0.85	3.52
B	0.83	3.47	0.84	3.52
C	0.82	3.47	0.83	3.42
	Roll Angle (deg)			
Case	**RMS Error**	**Max. Error**	**RMS Error**	**Max. Error**
A	0.76	2.25	0.79	2.62
B	1.19	3.35	0.80	2.38
C	1.42	3.70	0.80	2.41
Case	Non-transmission Rate (%)			
A	72.66		76.25	
B	79.6		82.77	
C	79.63		82.77	

Tables VI and VII show the comparative results in terms of the RMS error, maximum error, and non-transmission rate between the traditional and integral-based event-triggered mechanisms during the driving maneuvers. The results show that the integral-based event-triggered mechanism reduces the number of data transmitted over the network in comparison with the traditional event-triggered mechanism, by up to 7% and 5% for the Mercedes Sprinter van and the GOKA 650, respectively, with similar performance in terms of estimation of the vehicle angles. Figures 6 and 7 show time-based plots of the simulated and estimated sideslip and roll angles, and the release instants for the traditional and integral-based event-triggered mechanisms. The experimental results confirm the effectiveness of the proposed observer.

The observer was implemented in C++ and executed on a Raspberry Pi with a 1.4-GHz ARM processor connected to the internet via WiFi. The computation time of the proposed observer is relatively short, less than 0.1 ms per cycle, which ensures its execution in real time.

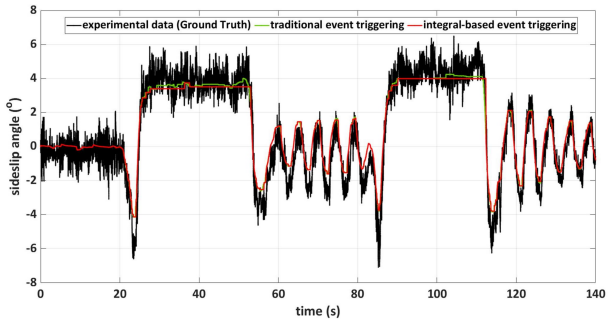

(a) Sideslip angle

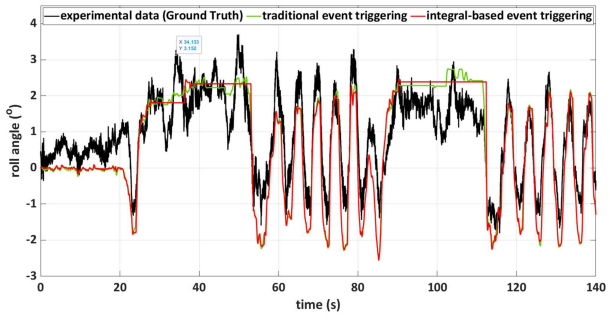

(b) Roll angle

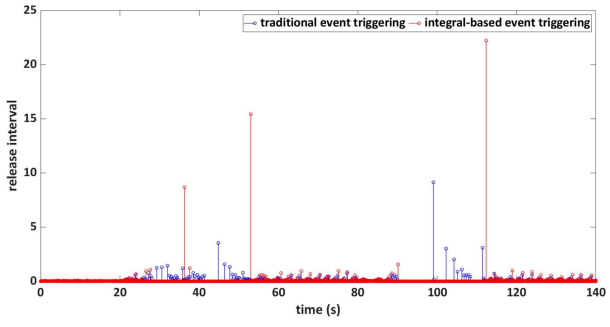

(c) Release instants

Fig. 6. Mercedes Sprinter van: experimental results for case A

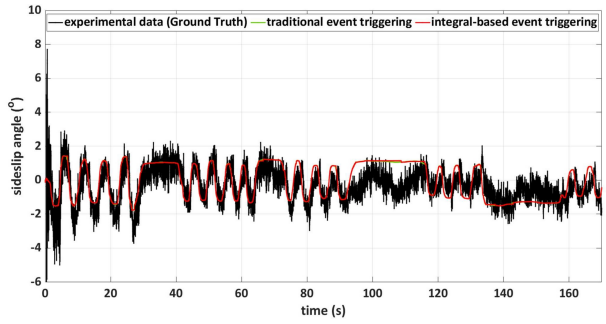

(a) Sideslip angle

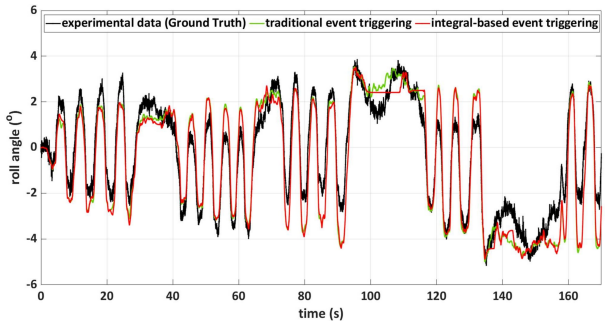

(b) Roll angle

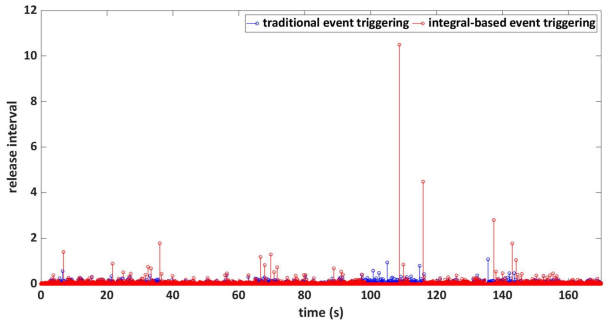

(c) Release instants

Fig. 7. GOKA 650: experimental results for case A

TABLE VII
EXPERIMENTAL RESULTS FOR THE GOKA 650: CASE B

Traditional Event Triggering		**Integral-Based Event Triggering**	
Sideslip Angle (deg)			
RMS Error	**Max. Error**	**RMS Error**	**Max. Error**
0.91	11.44	0.91	11.44
Roll Angle (deg)			
RMS Error	**Max. Error**	**RMS Error**	**Max. Error**
0.89	2.76	0.88	2.63
Non-transmission Rate (%)			
73.20		76.89	

V. CONCLUSION

An integral-based event-triggered H_∞ observer to simultaneously estimate the sideslip and roll angles, considering intravehicle communications with a networked-induced delay, is proposed herein. Based on an augmented Lyapunov–Krasovskii functional, sufficient conditions on the design of the integral-based event-triggered parameters and the observer to achieve global asymptotic stability are established in terms of linear matrix inequalities. As the longitudinal velocity and tire cornering stiffness of the vehicle have a strong influence on its lateral stability and can vary significantly when driving the vehicle, these time-varying parameter uncertainties were considered in the design of the observer. The simulation and experimental results and the robustness analysis show that the performance of the proposed integral-based event-triggered observer is better than that of the observer that uses a traditional event-triggered mechanism, in terms of the number of data transmitted over the communication network, with similar performance in the estimation of the vehicle angles. The results confirm that the proposed observer can improve the effective usage of the networked system, being able to reduce the data transmission over the network by up to 12%. Therefore, it is deemed more efficient in terms of the utilization of limited bandwidth.

APPENDIX A
PROOF OF THEOREM 1

Let us choose a candidate Lyapunov–Krasovskii functional as follows:

$$V(t) = V_1(t) + V_2(t) + V_3(t) + V_4(t), \tag{21}$$

where

$$V_1(t) = \xi^T(t)\mathbf{P}\xi(t), \tag{22}$$

$$V_2(t) = \sum_{i=1}^{N}\alpha_i\Big[\int_{t-\eta_m}^{t}\xi^T(s)\mathbf{Q}_{1,i}\xi(s)ds + \int_{t-\bar{\eta}}^{t-\eta_m}\xi^T(s)\mathbf{Q}_{2,i}\xi(s)ds\Big], \tag{23}$$

$$V_3(t) = \sum_{i=1}^{N}\alpha_i\Big[\eta_m\int_{-\eta_m}^{0}\int_{t+\theta}^{t}\dot{\xi}^T(s)\mathbf{R}_{1,i}\dot{\xi}(s)dsd\theta + (\bar{\eta}-\eta_m)\int_{-\bar{\eta}}^{-\eta_m}\int_{t+\theta}^{t}\dot{\xi}^T(s)\mathbf{R}_{2,i}\dot{\xi}(s)dsd\theta\Big], \tag{24}$$

$$V_4(t) = (\bar{\eta}-\eta)\, e_y^T(t)\mathbf{Z}e_y(t), \tag{25}$$

with $\bar{\eta} = h + \eta_M$.

The derivative $\dot{V}(t)$ with respect to t along the trajectory of system (17) can be written as

$$\dot{V}(t) = \dot{V}_1(t) + \dot{V}_2(t) + \dot{V}_3(t) + \dot{V}_4(t), \tag{26}$$

where

$$\dot{V}_1(t) = \dot{\xi}^T(t)\mathbf{P}\xi(t) + \xi^T(t)\mathbf{P}\dot{\xi}(t), \tag{27}$$

$$\dot{V}_2(t) = \sum_{i=1}^{N}\alpha_i\Big[\xi^T(t)\mathbf{Q}_{1,i}\xi(t) + \xi^T(t-\eta_m)\left(\mathbf{Q}_{2,i}-\mathbf{Q}_{1,i}\right) \times\xi(t-\eta_m) - \xi^T(t-\bar{\eta})\mathbf{Q}_{2,i}\xi(t-\bar{\eta})\Big], \tag{28}$$

$$\dot{V}_3(t) = \eta_m^2\dot{\xi}^T(t)\mathbf{R}_1\dot{\xi}(t) + (\bar{\eta}-\eta_m)^2\dot{\xi}^T(t)\mathbf{R}_2\dot{\xi}(t) - \eta_m\int_{t-\eta_m}^{t}\dot{\xi}^T(s)\mathbf{R}_1\dot{\xi}(s)ds - (\bar{\eta}-\eta_m)\int_{t-\bar{\eta}}^{t-\eta_m}\dot{\xi}^T(s)\mathbf{R}_2\dot{\xi}(s)ds, \tag{29}$$

$$\dot{V}_4(t) = -\mathbf{e}_y^T(t)\mathbf{Z}\mathbf{e}_y(t). \tag{30}$$

Applying Lemmas 1 and 2, on integration in $\dot{V}_3(t)$ and if LMI (20) holds, we get

$$\begin{aligned}\dot{V}_3(t) \le{}& \eta_m^2\dot{\xi}^T(t)\mathbf{R}_1\dot{\xi}(t) + (\bar{\eta}-\eta_m)^2\dot{\xi}^T(t)\mathbf{R}_2\dot{\xi}(t)\\ &-\Big(\xi(t)-\xi(t-\eta_m)\Big)^T\mathbf{R}_1\Big(\xi(t)-\xi(t-\eta_m)\Big)\\ &-\Big(\xi(t-\eta_m)-\xi(t-\eta)\Big)^T\mathbf{R}_2\Big(\xi(t-\eta_m)\xi(t-\eta)\Big)\\ &-\Big(\xi(t-\eta)-\xi(t-\bar{\eta})\Big)^T\mathbf{R}_2\Big(\xi(t-\eta)-\xi(t-\bar{\eta})\Big)\\ &+\Big(\xi(t-\eta_m)-\xi(t-\eta)\Big)^T\mathbf{S}^T\Big(\xi(t-\eta)-\xi(t-\bar{\eta})\Big)\\ &+\Big(\xi(t-\eta)-\xi(t-\bar{\eta})\Big)^T\mathbf{S}\Big(\xi(t-\eta_m)-\xi(t-\eta)\Big).\end{aligned} \tag{31}$$

From Lemma 1, the upper bound of inequality (11) is

$$\begin{aligned}&\frac{\epsilon^2}{h_M}\left(\int_{t-h_M}^{t}\big(\mathbf{e}_y(s)+\mathbf{C}\mathbf{x}\left(s-\eta\right)\big)ds\right)^T\Omega\\ &\qquad\times\int_{t-h_M}^{t}\big(\mathbf{e}_y(s)+\mathbf{C}\mathbf{x}\left(s-\eta\right)\big)ds\\ &-\frac{1}{h_M}\left(\int_{t-h_M}^{t}\mathbf{e}_y(s)ds\right)^T\Omega\int_{s-h_M}^{t}\mathbf{e}_y(s)ds\le 0.\end{aligned} \tag{32}$$

According Definition 1, the observer defined in (14) and (15) is asymptotically stable with H_∞ performance under the integral-based event-triggering condition (32), if the following inequality is satisfied

$$\begin{aligned}&\dot{V}_1(t)+\dot{V}_2(t)+\dot{V}_3(t)+\dot{V}_4(t)\\ &\quad+\frac{\epsilon^2}{h_M}\left(\int_{t-h_M}^{t}\left(\mathbf{e}_y(t)+\mathbf{\Theta}\xi(t-\eta)\right)dt\right)^T\Omega\\ &\qquad\times\left(\int_{t-h_M}^{t}\left(\mathbf{e}_y(t)+\mathbf{\Theta}\xi(t-\eta)\right)dt\right)\\ &-\frac{1}{h_M}\left(\int_{t-h_M}^{t}\mathbf{e}_y(s)ds\right)^T\Omega\left(\int_{t-h_M}^{t}\mathbf{e}_y(s)ds\right)\\ &\qquad+\xi^T(t)\mathbf{C}_1^T\mathbf{C}_1\xi(t)-\gamma\mathbf{q}^T(t)\mathbf{q}(t)\le 0.\end{aligned} \tag{33}$$

Substituting (27)–(30) into (33) and taking (31) into account, we get inequality (34), with $\Theta = \begin{bmatrix}\mathbf{0} & \mathbf{C}\end{bmatrix}$.

The inequality (34) can be rewritten as

$$\varsigma^T(t)\Pi\varsigma(t) + \varsigma(t)^T\Pi_1^T\mathbf{R}_1\Pi_1\varsigma(t) + \varsigma^T(t)\Pi_2^T\mathbf{R}_2\Pi_2\varsigma(t) < 0, \tag{35}$$

where $\varsigma(t) = \begin{bmatrix}\xi(t) & \xi(t-\eta) & \xi(t-\eta_m) & \xi(t-\bar{\eta}) & \mathbf{e}_y(t) & \mathbf{w}(t) & \int_{t-h_M}^{t}\xi(s-\eta)ds & \int_{t-h_M}^{t}e_y(s)ds\end{bmatrix}^T$ and

$$\Pi = \begin{bmatrix}\Pi_{11} & \Pi_{12} & \mathbf{R}_1 & \mathbf{0} & \Pi_{15} & \Pi_{16} & \mathbf{0} & \mathbf{0}\\ * & \Pi_{22} & \mathbf{R}_2+\mathbf{S} & \mathbf{R}_2+\mathbf{S}^T & \mathbf{0} & \mathbf{0} & \mathbf{0} & \mathbf{0}\\ * & * & \Pi_{33} & -\mathbf{S}^T & \mathbf{0} & \mathbf{0} & \mathbf{0} & \mathbf{0}\\ * & * & * & \Pi_{44} & \mathbf{0} & \mathbf{0} & \mathbf{0} & \mathbf{0}\\ * & * & * & * & -\mathbf{Z} & \mathbf{0} & \mathbf{0} & \mathbf{0}\\ * & * & * & * & * & -\gamma\mathbf{I} & \mathbf{0} & \mathbf{0}\\ * & * & * & * & * & * & \Pi_{55} & \Pi_{56}\\ * & * & * & * & * & * & * & \Pi_{66}\end{bmatrix},$$

$$\Pi_1 = \eta_m\sum_{i=1}^{N}\alpha_i\begin{bmatrix}\mathbf{A}_{0,i} & \mathbf{A}_{1,i} & \mathbf{0} & \mathbf{0} & \mathbf{A}_{2,i} & \mathbf{A}_{3,i} & \mathbf{0} & \mathbf{0}\end{bmatrix},$$

$$\Pi_2 = (\bar{\eta}-\eta_m)\sum_{i=1}^{N}\alpha_i\begin{bmatrix}\mathbf{A}_{0,i} & \mathbf{A}_{1,i} & \mathbf{0} & \mathbf{0} & \mathbf{A}_{2,i} & \mathbf{A}_{3,i} & \mathbf{0} & \mathbf{0}\end{bmatrix},$$

$$\sum_{i=1}^{N}\alpha_i\Big[\xi^T(t)\Big(\left(\mathbf{A}_{0,i}+\Delta\mathbf{A}_{0,i}\right)^T\mathbf{P}+\mathbf{P}\left(\mathbf{A}_{0,i}+\Delta\mathbf{A}_{0,i}\right)\Big)\xi(t)+\xi^T(t)\mathbf{P}\mathbf{A}_{1,i}\xi(t-\eta)+\xi^T(t)\mathbf{P}\mathbf{A}_{2,i}\mathbf{e}_y(t)$$
$$+\xi^T(t)\mathbf{P}\left(\mathbf{A}_{3,i}+\Delta\mathbf{A}_{3,i}\right)\mathbf{q}(t)+\xi^T(t-\eta)\mathbf{A}_{1,i}^T\mathbf{P}\xi(t)++\mathbf{e}_y^T(t)\mathbf{A}_{2,i}^T\mathbf{P}\xi(t)+\mathbf{q}^T(t)\left(\mathbf{A}_{3,i}+\Delta\mathbf{A}_{3,i}\right)^T\mathbf{P}\xi(t)\Big]$$
$$+\sum_{i=1}^{N}\alpha_i\Big[\xi^T(t)\mathbf{Q}_{1,i}\xi(t)+\xi^T(t-\eta_m)\left(\mathbf{Q}_{2,i}-\mathbf{Q}_{1,i}\right)\xi(t-\eta_m)-\xi^T(t-\bar{\eta})\mathbf{Q}_{2,i}\xi(t-\bar{\eta})\Big]+\eta_m^2\Big(\sum_{i=1}^{N}\alpha_i\Big[\left(\mathbf{A}_{0,i}+\Delta\mathbf{A}_{0,i}\right)\xi(t)$$
$$+\mathbf{A}_{1,i}\xi(t-\eta)+\mathbf{A}_{2,i}\mathbf{e}_y(t)+\left(\mathbf{A}_{3,i}+\Delta\mathbf{A}_{3,i}\right)\mathbf{q}(t)\Big]\Big)^T\mathbf{R}_1\Big(\sum_{i=1}^{N}\alpha_i\Big[\left(\mathbf{A}_{0,i}+\Delta\mathbf{A}_{0,i}\right)\xi(t)+\mathbf{A}_{1,i}\xi(t-\eta)+\mathbf{A}_{2,i}\mathbf{e}_y(t)$$
$$+\left(\mathbf{A}_{3,i}+\Delta\mathbf{A}_{3,i}\right)\mathbf{q}(t)\Big]\Big)\left(\bar{\eta}-\eta_m\right)^2\Big(\sum_{i=1}^{N}\alpha_i\Big[\left(\mathbf{A}_{0,i}+\Delta\mathbf{A}_{0,i}\right)\xi(t)+\mathbf{A}_{1,i}\xi(t-\eta)+\mathbf{A}_{2,i}\mathbf{e}_y(t)+\left(\mathbf{A}_{3,i}+\Delta\mathbf{A}_{3,i}\right)\mathbf{q}(t)\Big]\Big)^T\mathbf{R}_2$$
$$\times\Big(\sum_{i=1}^{N}\alpha_i\Big[\left(\mathbf{A}_{0,i}+\Delta\mathbf{A}_{0,i}\right)\xi(t)+\mathbf{A}_{1,i}\xi(t-\eta)+\mathbf{A}_{2,i}\mathbf{e}_y(t)+\left(\mathbf{A}_{3,i}+\Delta\mathbf{A}_{3,i}\right)\mathbf{q}(t)\Big]\Big)-\Big(\xi(t)-\xi(t-\eta_m)\Big)^T\mathbf{R}_1$$
$$\times\Big(\xi(t)-\xi(t-\eta_m)\Big)-\Big(\xi(t-\eta_m)-\xi(t-\eta)\Big)^T\mathbf{R}_2\Big(\xi(t-\eta_m)-\xi(t-\eta)\Big)-\Big(\xi(t-\eta)-\xi(t-\bar{\eta})\Big)^T\mathbf{R}_2$$
$$\times\Big(\xi(t-\eta)-\xi(t-\bar{\eta})\Big)+\Big(\xi(t-\eta_m)-\xi(t-\eta)\Big)^T\mathbf{S}^T\Big(\xi(t-\eta)-\xi(t-\bar{\eta})\Big)+\Big(\xi(t-\eta)-\xi(t-\bar{\eta})\Big)^T\mathbf{S}\Big(\xi(t-\eta_m)-\xi(t-\eta)\Big)$$
$$-\mathbf{e}_y^T(t)\mathbf{Z}\mathbf{e}_y(t)+\frac{\epsilon^2}{h_M}\left(\int_{t-h_M}^{t}\left(\mathbf{e}_y(s)+\mathbf{\Theta}\xi(s-\eta)\right)ds\right)^T\Omega\left(\int_{t-h_M}^{t}\left(\mathbf{e}_y(s)+\mathbf{\Theta}\xi(s-\eta)\right)ds\right)$$
$$-\frac{1}{h_M}\left(\int_{t-h_M}^{t}\mathbf{e}_y(s)ds\right)^T\Omega\left(\int_{t-h_M}^{t}\mathbf{e}_y(s)ds\right)+\xi^T(t)\mathbf{C}_1^T\mathbf{C}_1\xi(t)-\gamma\mathbf{q}^T\mathbf{q}\le 0. \quad (34)$$

with

$$\Pi_{11}=\sum_{i=1}^{N}\alpha_i\Big[\left(\mathbf{A}_{0,i}+\Delta\mathbf{A}_{0,i}\right)^T\mathbf{P}+\mathbf{P}\left(\mathbf{A}_{0,i}+\Delta\mathbf{A}_{0,i}\right)$$
$$+\mathbf{Q}_{1,i}-\mathbf{R}_1+\mathbf{C}_1^T\mathbf{C}_1\Big],$$
$$\Pi_{12}=\sum_{i=1}^{N}\alpha_i\mathbf{P}\mathbf{A}_{1,i},\ \Pi_{15}=\sum_{i=1}^{N}\alpha_i\mathbf{P}\mathbf{A}_{2,i},$$
$$\Pi_{16}=\sum_{i=1}^{N}\alpha_i\mathbf{P}\left(\mathbf{A}_{3,i}+\Delta\mathbf{A}_{3,i}\right),\ \Pi_{22}=-2\mathbf{R}_2-\mathbf{S}^T-\mathbf{S},$$
$$\Pi_{33}=\sum_{i=1}^{N}\alpha_i\Big[\left(\mathbf{Q}_{2,i}-\mathbf{Q}_{1,i}\right)-\mathbf{R}_1-\mathbf{R}_2\Big],$$
$$\Pi_{44}=\sum_{i=1}^{N}\alpha_i\Big[-\mathbf{Q}_{2,i}-\mathbf{R}_2\Big],\ \Pi_{55}=\frac{\epsilon^2}{h_M}\Big[\Theta^T\Omega\Theta\Big],$$
$$\Pi_{56}=\frac{\epsilon^2}{h_M}\Big[\Theta^T\Omega\Big],\ \Pi_{66}=\Big[-\frac{\Omega}{h_M}+\frac{\epsilon^2}{h_M}\Omega\Big]. \quad (36)$$

By the Schur complement, inequality (35) is equivalent to

$$\sum_{i=1}^{N}\alpha_i\begin{bmatrix}\Pi_i & \Pi_{1,i}^T & \Pi_{2,i}^T\\ * & -\mathbf{R}_1^{-1} & 0\\ * & * & -\mathbf{R}_2^{-1}\end{bmatrix}<0. \quad (37)$$

Inequality (37) is obeyed if the following condition is met for each of the terms:

$$\begin{bmatrix}\Pi_i & \Pi_{1,i}^T & \Pi_{2,i}^T\\ * & -\mathbf{R}_1^{-1} & 0\\ * & * & -\mathbf{R}_2^{-1}\end{bmatrix}<0,\ \text{for}\, i=1,\dots N. \quad (38)$$

Pre- and post-multiplying both sides of inequality (38) by $diag\{\mathbf{I},\mathbf{P},\mathbf{P}\}$, we have

$$\begin{bmatrix}\Pi_i & \Pi_{1,i}^T\mathbf{P} & \Pi_{2,i}^T\mathbf{P}\\ * & -\mathbf{P}\mathbf{R}_1^{-1}\mathbf{P} & \mathbf{0}\\ * & * & -\mathbf{P}\mathbf{R}_2^{-1}\mathbf{P}\end{bmatrix}<0. \quad (39)$$

Applying Lemma 3 to (39), we get

$$\begin{bmatrix}\Pi_i & \Pi_{1,i}^T\mathbf{P} & \Pi_{2,i}^T\mathbf{P}\\ * & \rho_1^2\mathbf{R}_1-2\rho_1\mathbf{P} & \mathbf{0}\\ * & * & \rho_2^2\mathbf{R}_2-2\rho_2\mathbf{P}\end{bmatrix}<0. \quad (40)$$

Using (4), noting that $\mathbf{M}_A^T\mathbf{M}_A\le\mathbf{I}$, $\mathbf{M}_{\mathbf{B}_\delta}^T\mathbf{M}_{\mathbf{B}_\delta}\le\mathbf{I}$, and $\mathbf{M}_{\mathbf{B}_u}^T\mathbf{M}_{\mathbf{B}_u}\le\mathbf{I}$ are satisfied, and reapplying the Schur complement, we obtain from (40) that

$$\begin{bmatrix}\bar{\mathbf{\Gamma}}_{11,i} & \mathbf{0} & \bar{\mathbf{\Gamma}}_{13,i} & \bar{\mathbf{\Gamma}}_{14,i} & \bar{\mathbf{\Gamma}}_{15,i}\\ * & \bar{\mathbf{\Gamma}}_{22,i} & \mathbf{0} & \mathbf{0} & \mathbf{0}\\ * & * & \bar{\mathbf{\Gamma}}_{33,i} & \bar{\mathbf{\Gamma}}_{34,i} & \bar{\mathbf{\Gamma}}_{35,i}\\ * & * & * & -\mu_1\mathbf{I} & \mathbf{0}\\ * & * & * & * & -\mu_2\mathbf{I}\end{bmatrix}<\mathbf{0}\ \ \text{for}\, i=1,2,\dots,N, \quad (41)$$

where

$$\bar{\Gamma}_{11,i} = \begin{bmatrix} \bar{\Gamma}_{11}^{11,i} & \bar{\Gamma}_{12}^{11,i} & \mathbf{R}_1 & \mathbf{0} & \bar{\Gamma}_{15}^{11,i} & \bar{\Gamma}_{16}^{11,i} \\ * & \bar{\Gamma}_{22}^{11,i} & \mathbf{R}_2+\mathbf{S} & \mathbf{R}_2+\mathbf{S}^T & \mathbf{0} & \mathbf{0} \\ * & * & \bar{\Gamma}_{33}^{11,i} & -\mathbf{S}^T & \mathbf{0} & \mathbf{0} \\ * & * & * & \bar{\Gamma}_{44}^{11,i} & \mathbf{0} & \mathbf{0} \\ * & * & * & * & -\mathbf{Z} & \mathbf{0} \\ * & * & * & * & * & -\gamma^2\mathbf{I} \end{bmatrix},$$

$\bar{\Gamma}_{11}^{11,i} = \mathbf{A}_{0,i}^T\mathbf{P} + \mathbf{P}\mathbf{A}_{0,i} + \mathbf{Q}_{1,i} - \mathbf{R}_1$, $\bar{\Gamma}_{12}^{11,i} = \mathbf{P}\mathbf{A}_{1,i}$,
$\bar{\Gamma}_{15}^{11,i} = \mathbf{P}\mathbf{A}_{2,i}$, $\bar{\Gamma}_{16}^{11,i} = \mathbf{P}\mathbf{A}_{3,i}$, $\bar{\Gamma}_{22}^{11,i} = -2\mathbf{R}_2 - \mathbf{S}^T - \mathbf{S}$,
$\bar{\Gamma}_{33}^{11,i} = \mathbf{Q}_{2,i} - \mathbf{Q}_{1,i} - \mathbf{R}_1 - \mathbf{R}_2$, $\bar{\Gamma}_{44}^{11,i} = -\mathbf{Q}_{2,i} - \mathbf{R}_2$,

$$\bar{\Gamma}_{12,i} = \begin{bmatrix} \mathbf{0}\ \mathbf{0}\ \mathbf{C}_1^T \\ \mathbf{0}\ \mathbf{0}\ \mathbf{0} \\ \mathbf{0}\ \mathbf{0}\ \mathbf{0} \\ \mathbf{0}\ \mathbf{0}\ \mathbf{0} \\ \mathbf{0}\ \mathbf{0}\ \mathbf{0} \\ \mathbf{0}\ \mathbf{0}\ \mathbf{0} \end{bmatrix}, \bar{\Gamma}_{13,i} = \begin{bmatrix} \eta_m\mathbf{A}_{0,i}^T\mathbf{P} & (\bar{\eta}-\eta_m)\,\mathbf{A}_{0,i}^T\mathbf{P} \\ \eta_m\mathbf{A}_{1,i}^T\mathbf{P} & (\bar{\eta}-\eta_m)\,\mathbf{A}_{1,i}^T\mathbf{P} \\ \mathbf{0} & \mathbf{0} \\ \mathbf{0} & \mathbf{0} \\ \eta_m\mathbf{A}_{2,i}^T\mathbf{P} & (\bar{\eta}-\eta_m)\,\mathbf{A}_{2,i}^T\mathbf{P} \\ \eta_m\mathbf{A}_{3,i}^T\mathbf{P} & (\bar{\eta}-\eta_m)\,\mathbf{A}_{3,i}^T\mathbf{P} \end{bmatrix},$$

$$\bar{\Gamma}_{14,i} = \begin{bmatrix} \mathbf{P}\bar{\mathbf{E}}_A & \bar{\mathbf{F}}_A^T \\ \mathbf{0} & \mathbf{0} \\ \mathbf{0} & \mathbf{0} \\ \mathbf{0} & \mathbf{0} \\ \mathbf{0} & \mathbf{0} \\ \mathbf{0} & \mathbf{0} \end{bmatrix}, \bar{\Gamma}_{15,i} = \begin{bmatrix} \mathbf{P}\bar{\mathbf{E}}_\mathbf{B} & \mathbf{0} \\ \mathbf{0} & \mathbf{0} \\ \mathbf{0} & \mathbf{0} \\ \mathbf{0} & \mathbf{0} \\ \mathbf{0} & \mathbf{0} \\ \mathbf{0} & \mu_2\bar{\mathbf{F}}_\mathbf{B}^T \end{bmatrix},$$

$$\bar{\Gamma}_{22,i} = \begin{bmatrix} \frac{\epsilon^2}{h_M}\Theta^T\Omega\Theta & \frac{\epsilon^2}{h_M}\Theta^T\Omega & \mathbf{0} \\ * & -\frac{\Omega}{h_M} + \frac{\epsilon^2}{h_M}\Omega & \mathbf{0} \\ * & * & -\mathbf{I} \end{bmatrix},$$

$$\bar{\Gamma}_{33,i} = \begin{bmatrix} \rho_1^2\mathbf{R}_1 - 2\rho_1\mathbf{P} & \mathbf{0} \\ * & \rho_2^2\mathbf{R}_2 - 2\rho_2\mathbf{P} \end{bmatrix},$$

$$\bar{\Gamma}_{34,i} = \begin{bmatrix} \eta_m\mathbf{P}\bar{\mathbf{E}}_\mathbf{A} & \mathbf{0} \\ (\bar{\eta}-\eta_m)\,\mathbf{P}\bar{\mathbf{E}}_\mathbf{A} & \mathbf{0} \end{bmatrix}, \bar{\Gamma}_{35,i} = \begin{bmatrix} \eta_m\mathbf{P}\bar{\mathbf{E}}_\mathbf{B} & \mathbf{0} \\ (\bar{\eta}-\eta_m)\,\mathbf{P}\bar{\mathbf{E}}_\mathbf{B} & \mathbf{0} \end{bmatrix}.$$

Finally, by assuming that the matrix $\mathbf{P}$ has the structure

$$\mathbf{P} = \begin{bmatrix} \mathbf{P}_1 & \mathbf{0} \\ \mathbf{0} & \mathbf{P}_2 \end{bmatrix},$$

and applying the transformation $\mathbf{M}_i = \mathbf{P}_1\mathbf{L}_i$, LMI (19) is obtained.

This completes the proof.

APPENDIX B
OBSERVER GAINS AND TRIGGERING PARAMETERS IN THE TRUCKSIM® ENVIRONMENT FOR THE TRADITIONAL EVENT-TRIGGERED MECHANISM

- Case A
  - First triangle of the polytope

$$\Omega_1 = \begin{bmatrix} 0.994 & 0 \\ 0 & 0.994 \end{bmatrix}, \mathbf{L_1} = \begin{bmatrix} 0.205 & -0.322 \\ -1.121 & 2.081 \\ -0.0183 & -0.027 \\ 0.459 & 1.330 \end{bmatrix},$$

$$\mathbf{L_2} = \begin{bmatrix} -0.071 & 0.167 \\ 2.545 & -1.828 \\ 0.006 & -0.117 \\ -0.893 & 5.598 \end{bmatrix}, \mathbf{L_3} = \begin{bmatrix} 1.191 & -2.013 \\ -10.710 & 13.105 \\ -0.035 & -0.005 \\ 2.569 & -0.240 \end{bmatrix}.$$

  - Second triangle of the polytope

$$\Omega_2 = \begin{bmatrix} 0.994 & 0 \\ 0 & 0.994 \end{bmatrix}, \mathbf{L_3} = \begin{bmatrix} 3.413 & 0.171 \\ -26.725 & -3.143 \\ -0.093 & -0.179 \\ 6.990 & 8.569 \end{bmatrix},$$

$$\mathbf{L_4} = \begin{bmatrix} 8.239 & -1.376 \\ -43.490 & 6.652 \\ -0.026 & -0.200 \\ 8.388 & 7.936 \end{bmatrix}, \mathbf{L_5} = \begin{bmatrix} 22.703 & -6.847 \\ -87.587 & 20.738 \\ -0.100 & -0.165 \\ 21.751 & 1.717 \end{bmatrix}.$$

- Case B
  - First triangle of the polytope

$$\Omega_1 = \begin{bmatrix} 22.630 & -1.512 \\ -1.512 & 8.888 \end{bmatrix}, \mathbf{L_1} = \begin{bmatrix} 0.250 & 2.281 \\ 3.472 & -12.433 \\ -0.070 & -1.207 \\ 8.094 & 234.330 \end{bmatrix},$$

$$\mathbf{L_2} = \begin{bmatrix} 0.116 & 2.034 \\ 4.492 & -12.367 \\ -0.007 & -1.244 \\ -3.999 & 230.554 \end{bmatrix},$$

$$\mathbf{L_3} = \begin{bmatrix} -0.768 & 1.026 \\ 5.874 & -10.660 \\ 0.044 & -1.203 \\ -16.569 & 223.186 \end{bmatrix}.$$

  - Second triangle of the polytope

$$\Omega_2 = \begin{bmatrix} 21.449 & -0.346 \\ -0.3463 & 8.232 \end{bmatrix}, \mathbf{L_3} = \begin{bmatrix} 1.482 & 6.394 \\ -1.165 & -2.470 \\ -0.036 & -1.319 \\ 6.350 & 117.708 \end{bmatrix},$$

$$\mathbf{L_4} = \begin{bmatrix} -0.598 & 6.162 \\ 1.234 & -2.057 \\ -0.002 & -1.387 \\ -2.245 & 116.812 \end{bmatrix}, \mathbf{L_5} = \begin{bmatrix} 1.482 & 6.394 \\ -1.165 & -2.470 \\ -0.036 & -1.319 \\ 6.350 & 117.708 \end{bmatrix}.$$

- Case C
  - First triangle of the polytope

$$\Omega_1 = \begin{bmatrix} 22.531 & -1.593 \\ -1.593 & 8.945 \end{bmatrix}, \mathbf{L_1} = \begin{bmatrix} 0.173 & 2.636 \\ 4.104 & -16.069 \\ -0.0520 & -0.967 \\ 7.492 & 262.736 \end{bmatrix},$$

$$\mathbf{L_2} = \begin{bmatrix} 0.034 & 2.362 \\ 5.330 & -15.818 \\ 0.004 & -1.000 \\ -6.633 & 258.222 \end{bmatrix}, \mathbf{L_3} = \begin{bmatrix} -0.921 & 1.321 \\ 7.097 & -13.670 \\ 0.043 & -0.968 \\ -21.619 & 250.489 \end{bmatrix}.$$

  - Second triangle of the polytope

$$\Omega_2 = \begin{bmatrix} 20.933 & -0.342 \\ -0.342 & 8.196 \end{bmatrix}, \mathbf{L_3} = \begin{bmatrix} 1.082 & 8.215 \\ -0.991 & -4.506 \\ -0.049 & -1.963 \\ 5.968 & 160.158 \end{bmatrix},$$

$$\mathbf{L_4} = \begin{bmatrix} -1.127 & 7.897 \\ 1.232 & -3.967 \\ -0.003 & -2.033 \\ -3.620 & 158.995 \end{bmatrix}, \mathbf{L_5} = \begin{bmatrix} -7.231 & 6.656 \\ 8.412 & -1.953 \\ 0.042 & -1.976 \\ -20.482 & 156.236 \end{bmatrix}.$$

REFERENCES

[1] Q. Lu, P. Gentile, A. Tota, A. Sorniotti, P. Gruber, F. Costamagna, and J. De Smet, "Enhancing vehicle cornering limit through sideslip and yaw rate control," *Mechanical Systems and Signal Processing*, vol. 75, pp. 455–472, 2016.

[2] J. Zhang, W. Sun, and Z. Feng, "Vehicle yaw stability control via H_∞-gain scheduling," *Mechanical Systems and Signal Processing*, vol. 106, pp. 62–75, 2018.

[3] S. Li, G. Wang, B. Zhang, Z. Yu, and G. Cui, "Vehicle yaw stability control at the handling limits based on model predictive control," *International Journal of Automotive Technology*, vol. 21, no. 2, pp. 361–370, 2020.

[4] K.-U. Henning, S. Speidel, F. Gottmann, and O. Sawodny, "Integrated lateral dynamics control concept for over-actuated vehicles with state and parameter estimation and experimental validation," *Control Engineering Practice*, vol. 107, p. 104704, 2021.

[5] Y. Ma, J. Chen, J. Wang, Y. Xu, and Y. Wang, "Path-tracking considering yaw stability with passivity-based control for autonomous vehicles," *IEEE Transactions on Intelligent Transportation Systems*, 2021.

[6] K. Ma, Z. Xie, P. K. Wong, W. Li, S. Chu, and J. Zhao, "Robust ts fuzzy fault tolerant control for vehicle lateral dynamics stabilization with integrated actuator fault and time delay," *Journal of Dynamic Systems, Measurement, and Control*, 2021.

[7] E. Sert and P. Boyraz, "Optimization of suspension system and sensitivity analysis for improvement of stability in a midsize heavy vehicle," *Engineering Science and Technology, an International Journal*, vol. 20, no. 3, pp. 997–1012, 2017.

[8] D. Chu, Z. Li, J. Wang, C. Wu, and Z. Hu, "Rollover speed prediction on curves for heavy vehicles using mobile smartphone," *Measurement*, vol. 130, pp. 404–411, 2018.

[9] L. Zhao and Z. Liu, "Vehicle velocity and roll angle estimation with road and friction adaptation for four-wheel independent drive electric vehicle," *Mathematical Problems in Engineering*, vol. 2014, 2014.

[10] D. Selmanaj, M. Corno, G. Panzani, and S. M. Savaresi, "Robust vehicle sideslip estimation based on kinematic considerations," *IFAC-PapersOnLine*, vol. 50, no. 1, pp. 14 855–14 860, 2017.

[11] B. L. Boada, M. J. L. Boada, L. Vargas-Melendez, and V. Diaz, "A robust observer based on H_∞ filtering with parameter uncertainties combined with neural networks for estimation of vehicle roll angle," *Mechanical Systems and Signal Processing*, vol. 99, pp. 611 – 623, 2018.

[12] M. Kamal Mazhar, M. J. Khan, A. I. Bhatti, and N. Naseer, "A novel roll and pitch estimation approach for a ground vehicle stability improvement using a low cost imu," *Sensors*, vol. 20, no. 2, p. 340, 2020.

[13] D. Chindamo, B. Lenzo, and M. Gadola, "On the vehicle sideslip angle estimation: A literature review of methods, models, and innovations," *Applied Sciences*, vol. 8, no. 3, 2018.

[14] F. Di Biase, B. Lenzo, and F. Timpone, "Vehicle sideslip angle estimation for a heavy-duty vehicle via extended kalman filter using a rational tyre model," *IEEE Access*, vol. 8, pp. 142 120–142 130, 2020.

[15] E. Villano, B. Lenzo, and A. Sakhnevych, "Cross-combined UKF for vehicle sideslip angle estimation with a modified Dugoff tire model: design and experimental results," *Meccanica*, pp. 1–16, 2021.

[16] H. Qi, N. Zhang, Y. Chen, and B. Tan, "A comprehensive tune of coupled roll and lateral dynamics and parameter sensitivity study for a vehicle fitted with hydraulically interconnected suspension system," *Proceedings of the Institution of Mechanical Engineers, Part D: Journal of Automobile Engineering*, vol. 235, no. 1, pp. 143–161, 2021.

[17] K. Cho, H. Son, Y. Wang, K. Nam, and S. Choi, "Vehicle side-slip angle estimation of ground vehicles based on a lateral acceleration compensation," *IEEE Access*, vol. 8, pp. 180 433–180 443, 2020.

[18] A. Hac, D. Nichols, and D. Sygnarowicz, "Estimation of vehicle roll angle and side slip for crash sensing," SAE Technical Paper, Tech. Rep., 2010.

[19] J. Zhao, X. Wang, Z. Liang, W. Li, X. Wang, and P. K. Wong, "Adaptive event-based robust passive fault tolerant control for nonlinear lateral stability of autonomous electric vehicles with asynchronous constraints," *ISA Transactions*, 2021.

[20] C. Sommer and F. Dressler, *Inter-vehicle communication*. Cambridge University Press, 2014, p. 38–105.

[21] J. E. Siegel, D. C. Erb, and S. E. Sarma, "A survey of the connected vehicle landscape—architectures, enabling technologies, applications, and development areas," *IEEE Transactions on Intelligent Transportation Systems*, vol. 19, no. 8, pp. 2391–2406, 2017.

[22] T.-Y. Huang, C.-J. Chang, C.-W. Lin, S. Roy, and T.-Y. Ho, "Delay-bounded intravehicle network routing algorithm for minimization of wiring weight and wireless transmit power," *IEEE Transactions on Computer-Aided Design of Integrated Circuits and Systems*, vol. 36, no. 4, pp. 551–561, 2016.

[23] M. Al-Saud, A. M. Eltamaly, M. A. Mohamed, and A. Kavousi-Fard, "An intelligent data-driven model to secure intravehicle communications based on machine learning," *IEEE Transactions on Industrial Electronics*, vol. 67, no. 6, pp. 5112–5119, 2019.

[24] X. Zhu, H. Zhang, B. Yang, and G. Zhang, "Cloud-based shaft torque estimation for electric vehicle equipped with integrated motor-transmission system," *Mechanical Systems and Signal Processing*, vol. 99, pp. 647–660, 2018.

[25] F. Milani, M. Foell, and C. Beidl, "A data-based approach to predict the response time of cloud-based vehicle functions," in *2019 IEEE International Conference on Connected Vehicles and Expo (ICCVE)*. IEEE, 2019, pp. 1–6.

[26] X. Ge, Q.-L. Han, X.-M. Zhang, and D. Ding, "Dynamic event-triggered control and estimation: a survey," *International Journal of Automation and Computing*, pp. 1–30, 2021.

[27] C. Nowzari, E. Garcia, and J. Cortés, "Event-triggered communication and control of networked systems for multi-agent consensus," *Automatica*, vol. 105, pp. 1–27, 2019.

[28] T. Li, X. Tang, J. Ge, and S. Fei, "Event-based fault-tolerant control for networked control systems applied to aircraft engine system," *Information Sciences*, vol. 512, pp. 1063–1077, 2020.

[29] C. Yang, J. Xia, J. H. Park, H. Shen, and J. Wang, "Sliding mode control for uncertain active vehicle suspension systems: an event-triggered H_∞ control scheme," *Nonlinear Dynamics*, vol. 103, no. 4, pp. 3209–3221, 2021.

[30] X.-M. Zhang and Q.-L. Han, "Event-triggered dynamic output feedback control for networked control systems," *IET Control Theory & Applications*, vol. 8, no. 4, pp. 226–234, 2014.

[31] F. Viadero-Monasterio, B. Boada, M. Boada, and V. Díaz, "H_∞ dynamic output feedback control for a networked control active suspension system under actuator faults," *Mechanical Systems and Signal Processing*, vol. 162, p. 108050, 2022.

[32] S. H. Mousavi, M. Ghodrat, and H. J. Marquez, "Integral-based event-triggered control scheme for a general class of non-linear systems," *IET Control Theory & Applications*, vol. 9, no. 13, pp. 1982–1988, 2015.

[33] W. Kwon, B. Koo, and S. Lee, "Integral-based event-triggered synchronization criteria for chaotic lur'e systems with networked PD control," *Nonlinear Dynamics*, vol. 94, no. 2, pp. 991–1002, 2018.

[34] H. Yu and F. Hao, "Input-to-state stability of integral-based event-triggered control for linear plants," *Automatica*, vol. 85, pp. 248–255, 2017.

[35] H. Li, J. Pan, X. Zhang, and J. Yu, "Integral-based event-triggered fault estimation and impulsive fault-tolerant control for networked control systems applied to underwater vehicles," *Neurocomputing*, vol. 442, pp. 36–47, 2021.

[36] H. Yu and F. Hao, "The existence of zeno behavior and its application to finite-time event-triggered control," *Science China Information Sciences*, vol. 63, no. 1, pp. 1–3, 2020.

[37] M. J. L. Boada, B. L. Boada, and H. Zhang, "Event-triggering H_∞-based observer combined with NN for simultaneous estimation of vehicle sideslip and roll angles with network-induced delays," *Nonlinear Dynamics*, 2021.

[38] H. Du, N. Zhang, and G. Dong, "Stabilizing vehicle lateral dynamics with considerations of parameter uncertainties and control saturation through robust yaw control," *IEEE Transactions on Vehicular Technology*, vol. 59, no. 5, pp. 2593–2597, 2010.

[39] H. S. Kim, Y. J. Hyun, and K. H. Nam, "Disturbance observer-based sideslip angle control for improving cornering characteristics of in-wheel motor electric vehicles," *International Journal of Automotive Technology*, vol. 19, no. 6, pp. 1071–1080, 2018.

[40] W. Liu and J. Huang, "Robust practical output regulation for a class of uncertain linear minimum-phase systems by output-based event-triggered control," *International Journal of Robust and Nonlinear Control*, vol. 27, no. 18, pp. 4574–4590, 2017.

[41] B. L. Boada, D. Garcia-Pozuelo, M. J. L. Boada, and V. Diaz, "A constrained dual Kalman filter based on pdf truncation for estimation of vehicle parameters and road bank angle: Analysis and experimental validation," *IEEE Transactions on Intelligent Transportation Systems*, vol. 18, no. 4, pp. 1006–1016, 2017.

[42] N. Zhang, Y. Zhang, H. Tian, Y. Li, and J. Hu, "State feedback control based on regional pole placement on handling stability of ground vehicles," *IEEE Access*, vol. 7, pp. 165 411–165 419, 2019.

[43] X. Zhang and Q. Han, "Event-triggered dynamic output feedback control for networked control systems," *IET Control Theory Applications*, vol. 8, no. 4, pp. 226–234, 2014.

[44] S. H. Mousavi, M. Ghodrat, and H. J. Marquez, "A novel integral-based event triggering control for linear time-invariant systems," in *53rd IEEE conference on decision and control*. IEEE, 2014, pp. 1239–1243.
[45] Z. Zhang and L. Wang, "Distributed integral-type event-triggered synchronization of multiagent systems," *International Journal of Robust and Nonlinear Control*, vol. 28, no. 14, pp. 4175–4187, 2018.
[46] J. Xiong and J. Lam, "Stabilization of networked control systems with a logic ZOH," *IEEE Transactions on Automatic Control*, vol. 54, no. 2, pp. 358–363, 2009.
[47] L. Vargas-Meléndez, B. L. Boada, M. J. L. Boada, A. Gauchía, and V. Díaz, "A sensor fusion method based on an integrated neural network and Kalman filter for vehicle roll angle estimation," *Sensors*, vol. 16, no. 9, 2016.